# Structure of even-even Sr isotopes with math xmlns="http://www.w3.org/1998/Math/MathML">mrow>mn>50/mn>mo>≤/mo>mi>N/mi>mo>≤/mo>mn>58/mn>/mrow>/math> neutrons

W. Urban, K. Sieja, T. Rząca-Urban, J. Wiśniewski, A. Blanc, M. Jentschel, P. Mutti, U. Köster, T. Soldner, G. de France, G. S. Simpson, C. A. Ur, A. G. Smith, and J. P. Greene

Phys. Rev. C **104**, 064309 — Published 13 December 2021

DOI: 10.1103/PhysRevC.104.064309

# Structure of even-even Sr isotopes with 50≤N≤58 neutrons.

W. Urban,[1] K. Sieja,[2] T. Rząca-Urban,[3] J. Wiśniewski,[3] A. Blanc,[4] M. Jentschel,[4] P. Mutti,[4] U. Köster,[4] T. Soldner,[4] G. de France,[5] G. S. Simpson,[6] C.A. Ur,[7] A.G. Smith,[8] and J.P. Greene[9]

[1]*Faculty of Physics, University of Warsaw, PL-02-093 Warsaw, Poland*
[2]*Université de Strasbourg, IPHC, Strasbourg, France; CNRS, UMR7178, 67037 Strasbourg, France*
[3]*Faculty of Physics, University of Warsaw, ulica PL-02-093 Warsaw, Poland*
[4]*Institut Laue-Langevin, Grenoble, France*
[5]*Grand Accélérateur National d'Ions Lourds (GANIL), CEA/DSM - CNRS/IN2P3, Bd Henri Becquerel, BP 55027, F-14076 Caen Cedex 5, France*
[6]*LPSC, Université Joseph Fourier Grenoble 1, CNRS/IN2P3, Institut National Polytechnique de Grenoble, F-38026 Grenoble Cedex, France*
[7]*INFN, Legnaro, Italy*
[8]*Department of Physics and Astronomy, The University of Manchester, M13 9PL Manchester, UK*
[9]*Argonne National Laboratory, Argonne, IL 60439, USA*

(Dated: November 24, 2021)

Excited levels in $^{90}$Sr, $^{92}$Sr, $^{94}$Sr and $^{96}$Sr nuclei were reinvestigated using high-statistics multiple-$\gamma$ coincidence data from neutron-induced fission of $^{235}$U and spontaneous fission of $^{252}$Cf, measured using EXILL and Gammasphere arrays, respectively. The experimental goal was the search for new excited levels and firm spin-parity assignments to known levels. Total of 23 new levels with 30 new or corrected decays and 39 new or improved spin-parity assignments were obtained in the four nuclei. Negative-parity structures on top of $3^-$ excitation were firmly identified and extended to higher spins. New positive-parity structures in $^{94}$Sr and $^{96}$Sr were observed with $3^+$ excitations characteristic of $\gamma$ collectivity. The 277.7-keV, E2 decay from the 1507.0-keV level to the *second* $0^+$ level in $^{96}$Sr, found in this work, completes the coexisting deformed band in this nucleus. To learn about the microscopic structure of levels in the $^{88-96}$Sr nuclei we performed Large-Scale, Shell-Model (LSSM) calculations. The calculations compared to the experiment, helped the discussion of the evolution of collectivity in strontium isotopes, highlighting the important role of various single particle excitations in phase transitions and shape coexistence in the region. Special role of the neutron $9/2^+[404]$ extruder as a catalyst of the deformation change in the region is highlighted.

PACS numbers: 21.10.Tg, 23.20.Lv, 25.85.Ec, 27.60.+j

## I. INTRODUCTION

In a recent work [1] regular systematics of excitation energies of low-lying, $0^+$ levels in the neutron-rich nuclei of the mass A≈100 region were reported. Most of these levels follow smooth trends, but a few of them deviate from the pattern, as shown in Fig. 6 of that work. The deviations are observed in Sr and Zr isotopes, where the most pronounced and rapid shape-change phenomena in the region are observed. It is likely that the deviating levels are associated with coexisting shapes [2] and the observed deviations may provide an extra information on the shape evolution and coexistence in the region.

As illustrated in Fig. 1, the $0_2^+$ excitations in Ru isotopes lower their energies with the increasing neutron number in a way suggesting strong interaction between $0_1^+$ and $0_2^+$ levels, pointing to a collective character of $0_2^+$ levels [3]. In contrast, $0_2^+$ excitations in Sr vary their energies in a way, which suggests very weak interaction between $0_1^+$ and $0_2^+$ levels. This weakness is dramatically highlighted by the 215.4 keV excitation energy of the $0_2^+$ level in $^{98}$Sr [5], the lowest among $0_2^+$ levels in all even-even nuclei. The proximity of $0_1^+$ and $0_2^+$ levels in $^{98}$Sr with a well deformed ground state, suggests that the $0_2^+$ state has a different and rather non-collective nature.

It was proposed [1] that the $\nu 9/2[404]$ extruder orbital is involved in both, the rapid increase of the deformation in Sr and Zr isotopes at the neutron number N≈59 and the appearance of the $0_2^+$ level at an extraordinary low excitation energy in $^{98}$Sr and $^{100}$Zr. This picture is backed by analogous observations around neutron number N=90 in mass A≈150 region, another place where a sudden on-

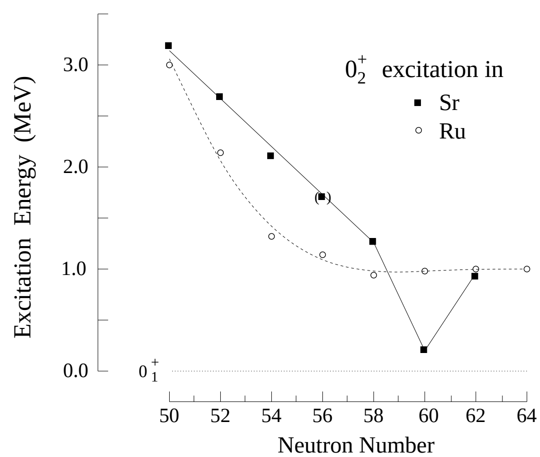


FIG. 1: Excitation energies of $0_2^+$ levels in Sr (full squares) and Ru (open dots) isotopes. The data are taken from Refs. [3, 4]. Lines are drawn to guide the eye.

set of deformation is observed. As shown in Refs. [6, 7], it is the $\nu 11/2[505]$ extruder orbital, which is involved in the rapid increase of the deformation in the A≈150 region. The recent work [8] proposed, in addition, an involvement of the *proton* 9/2[404] extruder in the process and suggested that the action of extruder orbitals is not limitted to passing of a single nucleon pair to a deformation-driving orbital (an effect proposed already at the advent of the Nilsson scheme [9]) but may be a multiple action. In this scenario the upslopping extruder acts as a catalyst of the deformation process, crossing a number of deformation-driving, down-slopping orbitals and passing and acquiring again pairs of nucleons, as the Fermi level increases with the increasing nucleon number. Such a multiple action has been considered theoretically within the "pair-hopping" model [10–12].

The two, very different patterns of the deformation onset shown in Fig.1 suggest that there is more than one mechanism involved in this process. As discussed in Refs. [12–17], the structure of transitional nuclei can be depicted as a "skeleton" of quasi-particle excitations in a self-consistent potential, "dressed" by various collective modes arising from both, residual interactions between valence nucleons as well as from quantum fluctuations of the potential. There are also other quantum effects present in such nuclei like restoring broken symmetries of the potential through nuclear rotation or mixing coexisting configurations through quantum tunneling.

Uncovering these effects and mechanisms requires detailed knowledge of nuclear excitations in chains of isotopes and isotones and, above all, knowing their spins and parities, which are fundamental quantum observable of nuclear systems in the laboratory frame. Such information helps tracing the characteristic excitations associated with various modes contributing to the development of collectivity in ground states as well as excited $0^+$ configurations.

The purpose of the present work is to update spectroscopic information on excited states in even Sr isotopes with 52≤N≤58 in order to identify basic excitations building the $0^+$ and other collective levels. Compared to our previous study of even-even Sr isotopes [18], based on the Eurogam measurement of prompt-$\gamma$ radiation following spontaneous fission of $^{248}$Cm [19], the present work uses prompt-$\gamma$ data of much higher statistics obtained from measurements of spontaneous fission of $^{252}$Cf and neutron-induced fission of $^{235}$U, respectively.

In Sec. II of the paper the measurements and results are presented and compared with previous works, with special emphasis on spin-parity assignments. In Sec. III we present a phenomenological description of the results and use the Large-Scale Shell-Model (LSSM) calculations to identify various excitation modes and trace their evolution in Sr isotopes. Section IV provides the summary and the outlook.

TABLE I: Relative intensities of strong, triple-$\gamma$ cascades in Sr isotopes, as observed in the Eurogam, Gammasphere and EXILL measurements [18, 20, 21], respectively.

| Isotope | Eurogam $^{248}$Cm fission | Gammasphere $^{252}$Cf fission | EXILL $^{235}$U+n fisison | Cascade (keV) |
|---|---|---|---|---|
| $^{90}$Sr | 0.005 | 0.20 | 1.0 | 831-824-1271 |
| | 0.003 | 0.16 | 1.0 | 831-824-2128 |
| | 0.007 | 0.17 | 1.0 | 831-824-314 |
| $^{92}$Sr | 0.075 | 0.24 | 1.0 | 815-859-1093 |
| | 0.050 | 0.32 | 1.0 | 815-1371-581 |
| $^{94}$Sr | 0.13 | 0.22 | 1.0 | 837-1309-1010 |
| | 0.14 | 0.29 | 1.0 | 837-1089-678 |
| $^{96}$Sr | 0.35 | 0.47 | 1.0 | 815-978-674 |
| | 0.36 | 0.45 | 1.0 | 815-978-993 |

## II. MEASUREMENTS AND RESULTS

New experimental results on $^{90}$Sr, $^{92}$Sr, $^{94}$Sr and $^{96}$Sr nuclei were obtained from measurements of $\gamma$ rays following spontaneous fission of $^{252}$Cf and neutron-induced fission of $^{235}$U, performed using Gammasphere [20] and EXILL [21] arrays of Anti-Compton Spectrometers (ACS), respectively. The two experiments provided significantly higher number of triple-$\gamma$ coincidences, compared to the Eurogam study [18], especially for $^{90,92}$Sr isotopes. Relative intensities of strong, triple-$\gamma$ cascades, as seen in the Eurogam, Gammasphere and EXILL measurements are presented in Table I. The present work is based predominantly on the EXILL data, with the Gammasphere data used as a counter-check.

The present study focuses on two experimental aspects, the identification of key, collective excitations mentioned in the Introduction and a reliable spin-parity assignments. The assignments are helped by new angular-correlations techniques for the EXILL [21] and $^{252}$Cf fission data [22], as well as new techniques for directional-polarization correlations using EXILL [23].

### A. Excitations in $^{90}$Sr

Low-spin levels of $^{90}$Sr were studied before in $\beta^-$ decay of the $0^-$ ground state and the $3^-$ isomer of $^{90}$Rb [24]. Medium-spin excitations were studied in heavy-ion-induced reactions [25, 26]. In the present work we observe weak prompt-$\gamma$ population of $^{90}$Sr levels in the neutron-induced fission (not competitive to Refs. [25, 26]) and a strong population in $\beta^-$ decay of $^{90}$Rb, produced either in fission or in $\beta^-$ decay of its isobars. Our triple-coincidence analysis provided results competitive to Ref. [24] and we confirm most of the levels with spin I≤5 listed in the compilation [27]. The quality of the coincidence data from EXILL is illustrated in Fig. 2, which shows examples of $\gamma$ spectra doubly-gated on strong lines of

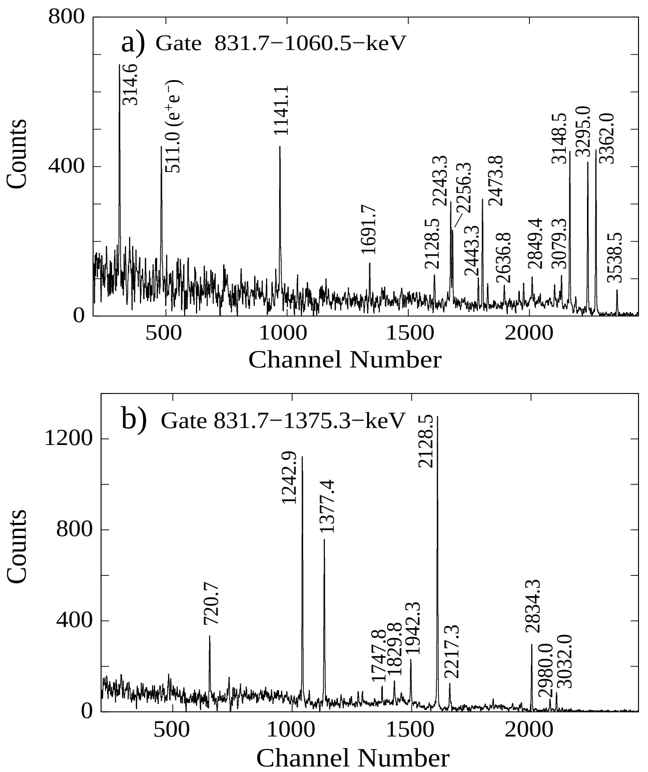


FIG. 2: Coincidence $\gamma$ spectra doubly gated on lines of $^{90}$Sr, as observed in the present work. Some known lines of $^{90}$Sr [24] seen in the figure are not listed in Table II.

$^{90}$Sr.

Table II lists all known levels in $^{90}$Sr up to of 3 MeV and those high-energy levels where new information was obtained in this work. Only transitions and decay branching, which are observed in coincidence spectra gated above the level in question, are shown. New results are marked in Table II with asterisk.

Spins and parities of levels in $^{90}$Sr are obtained from angular-correlation and directional-polarization-correlation measurements preformed using EXILL. The results are listed in Tables III and IV, respectively. All results in Table IV are new.

Figure 3 shows partial excitation scheme of $^{90}$Sr. Only levels and transitions discussed in the text are shown.

Spins and parities of 831.70-, 1655.95-, 1892.3-keV and 2497.3-keV levels reported in the compilation [27] are confirmed. We note the significantly higher 2497.4-keV branching from the 2497.3-keV level. The level at 2586(1) keV reported in [27] is not observed in the present work.

To the 2207.0-keV level we assign spin-parity $3^-$. The $\chi^2$-test value for this assignment is an order of magnitude smaller than for the $2^+$ spin-parity hypothesis. Very weak decays between this level and other negative-parity levels (see Refs. [25, 26]) suggest different structures.

To the 2528.1-keV level we assign positive parity. The $3^-$ hypothesis [27] is not confirmed, coinciding with the lack of decays from $4^-$ and $5^-$ levels [25, 26]. The $3^+$ assignment fits best the data but the $4^+$ is also possible.

To the 2571.0-keV level we assign spin-parity I=$3^{(+)}$. The large mixing ratio $\delta$=8.9 fits better the angular-correlation data than the other solution with $\delta$=-0.06.

The 1842.1-keV decay of the 2673.8-keV level is confirmed. Angular correlations support the $0^+$ spin-parity assignment to this level[27] because of the very large $A_4/A_0$ value, the unique feature of a 0-2-0 cascade.

The 2927.7-keV level has spin I=4, the only value consistent with angular correlations for both transitions depopulating this level and their branching. No decay to the $2^+$ level at 831.70 keV favors negative parity.

Our angular correlation data support the $0^+$ spin-parity of the 2971.1-keV level [27].

TABLE II: Energies, $E_i$ and spin-parities, $I_i^\pi$ of excited states in $^{90}$Sr with energies, $E_\gamma$ and $\gamma$-ray branching ratios, $I_\gamma$ for $\gamma$ decays as observed in this work. Levels and decays which are new or differ from the compilation [27] are marked with an asterisk. $E_f$ and $I_f^\pi$ denote the energy and spin-parity of levels populated by $\gamma$ decays listed in the third column.

| $E_i$ (keV) | $I_i^\pi$ | $E_\gamma$ (keV) | $I_\gamma$ (rel.) | $E_f$ (keV) | $I_f^\pi$ |
|---|---|---|---|---|---|
| 831.70(5) | $2^+$ | 831.70(5) | | 0.0 | $0^+$ |
| 1655.95(8) | $4^+$ | 824.25(5) | | | $2^+$ |
| 1892.3(1) | $2^+$ | 1060.50(5) | 100(3) | 831.70 | $2^+$ |
| | | 1892.5(3) | 8(1) | 0.0 | $0^+$ |
| 2207.0(1) | $3^-$ * | 314.6(1) | 5.1(7) | 1892.3 | $2^+$ |
| | | 551.2(2) | 4.9(7) | 1655.95 | $4^+$ |
| | | 1375.30(5) | 100(3) | 831.70 | $2^+$ |
| 2497.3(1) | $(2^+)$ | 1665.60(5) | 100(3) | 831.70 | $2^+$ |
| | | 2497.4(1) | 49(5) * | 0.0 | $0^+$ |
| 2528.1(2) | $3^+,4^+$ * | 872.4(1) | 55(15) | 1655.95 | $4^+$ |
| | | 1696.2(1) | 100(10) | 831.70 | $2^+$ |
| 2571.0(2) | $3^{(+)}$ * | 1739.3(1) | | 831.70 | $2^+$ |
| 2673.8(4) | $0^+$ * | 1842.1(3) | | 831.70 | $2^+$ |
| 2927.7(1) | $4^{(-)}$ | 720.7(1) | 15(5) * | 2207.0 | $3^-$ |
| | | 1271.7(1) | 100(5) | 1655.95 | $4^+$ |
| 2971.1(2) | $0^+$ | 2139.4(1) | | 831.70 | $2^+$ |
| 3449.8(1) | $2^+$ * | 952.7(1) | | 2497.3 | $(2^+)$ |
| | | 1242.90(5) | | 2207.0 | $3^-$ |
| | | 1793.9(1) | | 1665.95 | $4^+$ |
| | | 2617.7(3) | | 831.70 | $2^+$ |
| 3584.5(1) | $3^+$ * | 1377.4(2) | | 2207.0 | $3^-$ |
| | | 2752.80(5) | | 831.70 | $2^+$ |
| 4036.2(2) | $2^{(+)}$ * | 3204.5(1) | | 831.70 | $2^+$ |
| 4135.3(2) | $1,2^+$ | 3303.6(1) | | 831.70 | $2^+$ |
| 4148.8(1) | $3^+$ * | 1941.9(1) | | 2207.0 | $3^-$ |
| | | 2256.3(2) | | 1892.3 | $2^+$ |
| | | 3317.05(5) | | 831.70 | $2^+$ |
| 4335.4(2) | $3^+$ * | 3503.6(1) | | 831.70 | $2^+$ |
| | | 2128.5(1) | | 2207.0 | $3^-$ |
| 4366.1(2) | $1^+$ * | 3534.4(1) * | | 831.70 | $2^+$ |
| | | 2473.8(1) | | 1892.3 | $2^+$ |
| 4404.5(3) | 2,3 * | 3572.8(2) | | 831.70 | $2^+$ |
| 5430.6(3) * | | 3538.5(2) | | 1892.3 | $2^+$ |
| | | 4598.6(3) | | 831.7 | $2^+$ |

TABLE III: Angular correlation coefficients for $\gamma-\gamma$ cascades in $^{90}$Sr populated in neutron-induced fission of $^{235}$U. Label "sum" denotes summed correlations with all quadrupole transitions below the $E_{\gamma1}$.

| $E_{\gamma1}$-$E_{\gamma2}$ cascade | $A_2/A_0$ exp. | $A_4/A_0$ exp. | Spins in cascade | $\delta_{exp}(\gamma1)$ |
|---|---|---|---|---|
| 824.25 - 831.70 | 0.102(9) | 0.029(42) | 4 - 2 - 0 | |
| 1060.50 - 831.70 | -0.069(11) | 0.061(29) | 2 - 2 - 0 | 0.44(2) |
| | | | 3 - 2 - 0 | 0.003(16) |
| 1375.30 - 831.70 | -0.129(14) | 0.014(27) | 3 - 2 - 0 | -0.07(3) |
| | | | 2 - 2 - 0 | 0.53(2) |
| 1665.6 - 831.70 | 0.249(31) | 0.012(72) | 2 - 2 - 0 | 0.002(44) |
| | | | 3 - 2 - 0 | 0.7(+6,-2) |
| 1696.2 - 831.70 | 0.095(85) | -0.112(95) | 3 - 2 - 0 | 2.4 (4) |
| 1739.3 - 831.70 | -0.115(40) | -0.087(80) | 3 - 2 - 0 | 8.9(29) |
| | | | | or -0.06(5) |
| 1842.1 - 831.70 | -0.17(2) | 1.02(24) | 0 - 2 - 0 | |
| 2139.4 - 831.70 | 0.32(5) | 0.88(4) | 0 - 2 - 0 | |
| 2752.80 - 831.70 | 0.215(15) | -0.023(34) | 2 - 2 - 0 | 0.05(2) |
| | | | 3 - 2 - 0 | 0.50(5) |
| | | | | or 1.36(12) |
| 3204.5 - 831.70 | 0.012(66) | 0.39(14) | 2 - 2 - 0 | -9(4) |
| 3303.6 - 831.70 | -0.169(35) | 0.01(7) | 1 - 2 - 0 | -0.07(3) |
| | | | 2 - 2 - 0 | 0.60(8) |
| 3317.05 - 831.70 | 0.243(11) | 0.006(26) | 2 - 2 - 0 | 0.009(16) |
| | | | 3 - 2 - 0 | 0.62(7) |
| 3503.6 - 831.70 | 0.298(39) | 0.01(10) | 2 - 2 - 0 | -0.07(6) |
| | | | 3 - 2 - 0 | 0.83(26) |
| 3534.4 - 831.70 | -0.204(13) | -0.018(27) | 1 - 2 - 0 | 0.04(1) |
| | | | 3 - 2 - 0 | -0.17(2) |
| 3572.8 - 831.70 | 0.239(66) | 0.24(15) | 2 - 2 - 0 | -2.3(5) |
| | | | 3 - 2 - 0 | 0.6(2) |
| 2128.5 - 1375.30 | 0.84(30) | 0.06(6) | 3 - 3 - 2 | 0.7(1) |
| | | | | or -18(10) |
| 1271.7 - sum | 0.073(38) | -0.12(9) | 4 - 2 - 0 | 0.3(1) |
| 1793.9 - sum | 0.08(5) | 0.22(12) | 2 - 2 - 0 | -4.9(12) |

TABLE IV: Experimental, $P_{exp}(\gamma_1)$ and theoretical, $P_{th}(\gamma_1)$ values of linear polarization for the $\gamma_1$ (upper) transition in a $\gamma_1-\gamma_2$ cascade of $^{90}$Sr, as obtained from directional-polarization correlations in this work. The correlating, 831.70-keV $\gamma_2$ is assumed to be a $\Delta I$=2, E2 with $\delta$=0.

| $E_{\gamma1}$-$E_{\gamma2}$ | $P_{exp}(\gamma1)$ | Spin-parity | $\delta_{exp}(\gamma1)$ | $P_{th}(\gamma1)$ |
|---|---|---|---|---|
| 1060.50-831.70 | 0.34(7) | $2^+$ - $2^+$ - $0^+$ | 0.44(2) | 0.439(3) |
| | | $3^-$ - $2^+$ - $0^+$ | 0.003(16) | 0.105(6) |
| 1375.30-831.70 | 0.090(68) | $3^-$ - $2^+$ - $0^+$ | -0.07(3) | -0.076(7) |
| | | $2^+$ - $2^+$ - $0^+$ | 0.53(2) | 0.426(3) |
| 1665.60-831.70 | 0.14(17) | $2^+$ - $2^+$ - $0^+$ | 0.002(44) | 0.429(9) |
| | | $3^-$ - $2^+$ - $0^+$ | 0.7(+6,-2) | -0.43(9) |
| 2752.80-831.70 | -0.38(16) | $2^-$ - $2^+$ - $0^+$ | 0.05(2) | -0.430(4) |
| | | $3^+$ - $2^+$ - $0^+$ | 0.50(5) | -0.354(6) |
| 3317.75-831.70 | -0.50(15) | $2^-$ - $2^+$ - $0^+$ | 0.009(16) | -0.439(6) |
| | | $3^+$ - $2^+$ - $0^+$ | 0.62(7) | -0.404(7) |
| 3503.6-831.70 | -0.60(45) | $2^-$ - $2^+$ - $0^+$ | -0.07(6) | -0.409(8) |
| | | $3^+$ - $2^+$ - $0^+$ | 0.83(26) | -0.468(9) |
| 3534.4-831.70 | -0.19(17) | $1^+$ - $2^+$ - $0^+$ | 0.04(1) | -0.307(5) |
| | | $3^+$ - $2^+$ - $0^+$ | -0.17(2) | -0.045(9) |

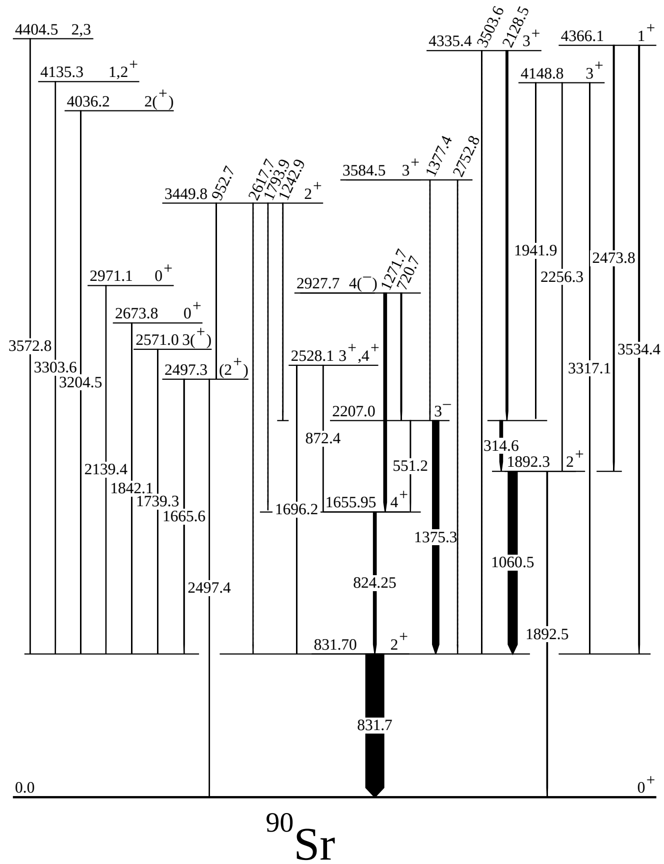


FIG. 3: Partial level scheme of $^{90}$Sr as seen in this work following fission of $^{235}$U induced by thermal neutrons. Arrow width is proportional to the observed $\gamma$ intensity.

Angular and directional-polarization correlations, for the 2752.8-831.7-keV cascade indicate spin-parity of $2^-$ or $3^+$ for the 3584.5-keV level. The $logft$ of 6.5 for this level, populated in $\beta^-$ decay of the $3^-$ isomer in $^{90}$Rb [27] and the observed branching favor spin-parity $3^+$.

For the 3449.8-keV level the present angular correlations uniquely indicate spin I=2. Positive parity is consistent with $logft$ of 6.9 for this level, populated in $\beta^-$ decay of the $3^-$ isomer in $^{90}$Rb [27] and the decay branching. Similarly, angular correlations uniquely indicate spin I=2 for the 4036.2-keV level. The decay branching for this level favors positive parity.

Angular correlations for the 3303.6-831.7-keV cascade are consistent with spin I=1 or I=2 for the 4135.3-keV level, also proposed in Ref. [27]. Large mixing ratio for the 2-2-0 hypothesis favors positive parity.

Angular and directional-polarization correlations for the new, 3503.6-831.7-keV cascade indicate spin-parity $2^-$ or $3^+$ for the 4335.4-keV level. The $logft$ of 6.2 for this level, populated in $\beta^-$ decay of the $3^-$ isomer in $^{90}$Rb [27] is consistent with spin-parity $3^+$. With such spin the 2128.5-keV transition has large mixing ratio.

The 5426.66-keV level reported in [27] does not exist.

Instead, the 3534.4-keV decay of this level reported in [27] as feeding the 1892.3-keV level, depopulates the 4366.1-keV level and feeds the 831.7-keV level while the 1892.3-keV level is fed by the 3538.5-keV transition seen in Fig. 2 (a). This confirms the 5430.6-keV level, reported in [27] as uncertain. Angular and directional-polarization correlations, for the new, 3534.4-831.7-keV cascade indicate spin-parity of $1^+$ or $3^+$ for the 4366.1-keV level. The $logft$ of 5.9 for this level, populated in $\beta^-$ decay of the $0^-$ ground state of $^{90}$Rb [27] is consistent with spin I=1. Therefore, we assign spin-parity $1^+$ to the 4366.1-keV level.

### B. Excitations in $^{92}$Sr

New information on $^{92}$Sr was obtained in this work from the EXILL measurement of prompt-$\gamma$ rays following fission of $^{235}$U. As shown in Table I the present measurement provided an order of magnitude more triple-$\gamma$ events compared to the measurement of $^{248}$Cm fission [18]. Apart from Ref. [18] medium-spin levels in $^{92}$Sr were also reported in Refs. [25, 26].

In contrast to $^{90}$Sr the population of excited levels in $^{92}$Sr in $\beta^-$ decay of $^{92}$Rb is low because of the 95% $\beta^-$ decay branch to the ground state of $^{92}$Sr. Therefore, the present $\beta^-$ decay data are not competitive to previous measurements, though we could observe most of the levels reported in the compilation [28].

Excited levels of $^{92}$Sr observed in this work are listed in Table V and shown in Fig. 4. Some of the decays reported in Ref. [28] are not seen in our work because of high background in fission data. Spins and parities of the 1385.3-, 1778.4-, 2140.8-keV and 2821.0-keV levels, shown in Fig. 4 are taken from Ref. [28]. Other spin-parity assignments are based on on angular-correlation and directional-polarization-correlation measurements preformed in this work and listed in Tables VI and VII, respectively.

Our data confirm the $2^+$ and $4^+$ spin-parity assignments to the 814.90- and 1673.80-keV levels, reported in Refs. [18, 28].

Angular correlations for the 1273.6-814.90-keV cascade from the 2088.6-keV level and for the 1712.1-814.90-keV cascade from the 2526.9-keV level are consistent with spin I=0 assignment to both levels. Positive parity is adopted after Ref. [28].

In Ref. [18] spin I=3 with a tentative negative parity was assigned the 2186.1-keV level. Our correlations allow spin I=2 or I=3. Spin I=3 is more likely considering the observed population of $^{92}$Sr in fission and the yrast-population argument [29]. Angular correlations indicate large mixing ratio for the 1371.3-keV transition, which would suggest its M1+E2 multipolarity. However, the directional-polarization correlations indicate an E1+M2 multipolarity for the 1371.3-keV transition, thus a negative parity for the 2186.2-keV level.

Angular correlations and directional-polarization correlations for the 1092.90-858.90-keV cascade are consistent with $4^+$ or $5^-$ spin-parity for the 2766.7-keV level. The $4^-$ hypothesis considered before [18] can be rejected. The yrast-population argument [29] favors the $5^-$ solution. This is consistent with the observed population of the yrast-cascade in $^{92}$Sr in heavy-ion reactions [25, 26].

For the 3015.5-, 3130.2-, 3364.2- and 3559.8-keV levels we propose spins and parities as shown in Fig. 4 based on their angular correlations and decay properties and taking into account the yrast-population argument [29].

The 3787.4-keV level was first assigned spin-parity $(6^+)$ [26] and later $(6^-,7^-)$ [18]. The observed intensities of $\gamma$ transitions together with the yrast-population argument suggest spin I=7 for this level. On the other hand, angular correlations for the 1020.8-580.7-keV cascade from this level are not consistent with either $7^- - 5^- - 3^-$

TABLE V: Experimental properties of excited levels in $^{92}$Sr populated in neutron-induced fission of $^{235}$U. New or improved information compared to previous works is marked with asterisks. Spin-parity with superscript "a" is adopted from Ref. [28]. Explanation of other symbols as in Table II.

| $E_i$ (keV) | $I_i^\pi$ | $E_\gamma$ (keV) | $I_\gamma$ (rel.) | $E_f$ (keV) | $I_f^\pi$ |
|---|---|---|---|---|---|
| 814.90(5) | $2^+$ | 814.90(5) | | 0.0 | $0^+$ |
| 1385.3(3) | $2^{+a}$ | 570.4(2) | | 814.90 | $2^+$ |
| | | 1385.3(2) | | 0.0 | $0^+$ |
| 1673.8(1) | $4^+$ | 858.90(5) | | 814.90 | $2^+$ |
| 1778.4(2) | $2^{+a}$ | 393.3(2) | | 1385.3 | $2^+$ |
| | | 963.4(2) | | 814.90 | $2^+$ |
| 2053.6(3) | $(2^+)^a$ | 1238.7(2) | | 814.90 | $2^+$ |
| 2088.6(4) | $0^{(+)}$ | 1273.6(3) | | 814.90 | $2^+$ |
| 2140.8(3) | $1^{+a}$ | 755.6(3) | | 1385.3 | $2^+$ |
| | | 1326.0(2) | | 814.90 | $2^+$ |
| 2186.2(2) * | $(2^+),3^-$ * | 512.5(3) | 10(3)* | 1673.8 | $4^+$ |
| | | 1371.3(1) * | 100(3)* | 814.90 | $2^+$ |
| 2526.9(2) | $0^+$ | 385.9(4) | 20(10) | 2140.8 | $1^+$ |
| | | 1712.1(2) | 100(15) | 814.90 | $2^+$ |
| 2766.7(2) | $(4^+),5^-$ * | 580.7(1) | 55(5) | 2186.2 | $(2^+),3^-$ |
| | | 1092.90(5) | 100(5) | 1673.8 | $4^+$ |
| 2783.9(2) | | 1398.7(2) | | 1385.3 | $2^+$ |
| | | 1968.8(2) | | 814.90 | $2^+$ |
| 2821.0(3) | $2^{(+)}),(1)^a$ | 2006.4(2) | | 814.90 | $2^+$ |
| 2925.5(5) | | 1251.7(4) | | 1673.8 | $4^+$ |
| 3015.5(3) | 5 * | 1341.7(2) | | 1673.8 | $4^+$ |
| 3130.2(3) * | $(6^+)$ | 1456.4(2) | | 1673.8 | $4^+$ |
| 3364.2(2) * | $(5^-)$ | 597.2(3) | 5(2) | 2766.7 | $(4^+),5^-$ |
| | | 1178.1(2) | 70(20) | 2186.2 | $(2^+),3^-$ |
| | | 1690.5(2) | 100(20) | 1673.8 | $4^+$ |
| 3559.8(3) * | (6) | 793.1(1) | | 2766.7 | $(4^+),5^-$ |
| 3787.4(3) * | $6,(7^-)$ | 771.8(2) | 20(7) | 3015.5 | 5 |
| | | 1020.8(1) | 100(5) | 2766.7 | $(4^+),5^-$ |
| 4023.7(3) * | $(7^-)$ | 236.1(3) | 60(20) | 3787.4 | $6,(7^-)$ |
| | | 659.6(2) | 100(10) | 3364.2 | $(5^-)$ |
| 4930.0(4) | $(8,9^-)$ | 1142.6(2) | | 3787.4 | $6,(7^-)$ |
| 5060.1(6) * | $(8,9^-)$ * | 1036.4(4) | | 4023.7 | $(7^-)$ |
| 5730.0(5) * | $(10,11^-)$* | 800.0(2) | | 4930.0 | $(8,9^-)$ |

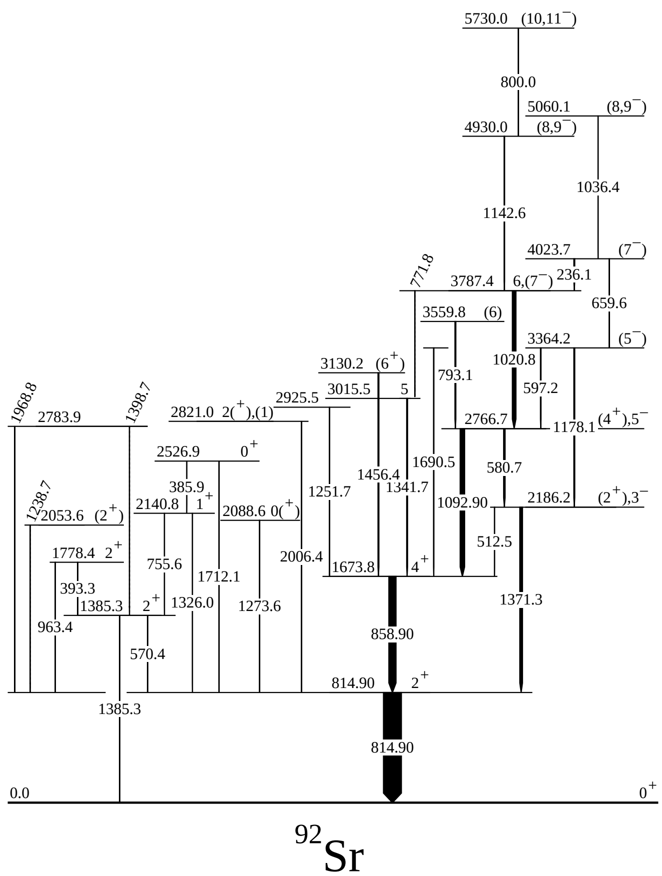


FIG. 4: Partial level scheme of $^{92}$Sr obtained in this work in measurements of $\gamma$ rays following neutron-induced fission of $^{235}$U. Arrow width is proportional to the observed $\gamma$ intensity.

TABLE VI: Angular correlation coefficients for $\gamma - \gamma$ cascades in $^{92}$Sr populated in neutron-induced fission of $^{235}$U. Label "sum" denotes summed correlations with all quadrupole transitions below the $E_{\gamma 1}$. Superscript "a" indicates mixed transition, if not $\gamma_1$.

| $E_{\gamma1}$-$E_{\gamma2}$ cascade | $A_2/A_0$ exp. | $A_4/A_0$ exp. | Spins in cascade | $\delta_{exp}(E_{\gamma1})$ |
|---|---|---|---|---|
| 580.7-1371.3$^a$ | -0.11(6) | 0.05(13) | 5 - 3 - 2 | -0.10(17) |
| | | | 5 - 3 - 2 | -2.8(11) |
| 1020.8-580.7 | -0.20(9) | -0.27(18) | | |
| 858.90-814.90 | 0.111(12) | -0.020(23) | 4 - 2 - 0 | |
| 1092.90-sum | 0.00(3) | 0.01(6) | 4 - 4 - 2 | 0.54(8) |
| | | | 5 - 4 - 2 | 0.11(4) |
| | | | 5 - 4 - 2 | 5.2(12) |
| 1273.6-814.90 | 0.91(61) | 0.75(13) | 0 - 2 - 0 | |
| 1341.7-sum | -0.13(9) | -0.29(19) | 5 - 4 - 2 | 90(-30,+200) |
| 1371.3-814.90 | 0.179(14) | -0.037(32) | 2 - 2 - 0 | 0.15(6) |
| | | | 3 - 2 - 0 | 0.35(5) |
| | | | 3 - 2 - 0 | 1.7(2) |
| 1456.4-sum | 0.095(60) | 0.04(18) | 6 - 4 - 2 | |
| 1712.1-814.90 | 0.16(7) | 0.80(15) | 0 - 2 - 0 | |

TABLE VII: Experimental, $P_{exp}(\gamma_1)$ and theoretical, $P_{th}(\gamma_1)$ values of linear polarization for the $\gamma_1$ (upper) transition in a $\gamma_1 - \gamma_2$ cascade of $^{92}$Sr, populated in neutron-induced fission of $^{235}$U, as obtained in this work. The correlating $\gamma_2$ of 814.90 keV is assumed to be a stretched, E2 transition with $\delta$=0. Label "p" indicates the transition for which the polarization was determined, if not $\gamma_1$.

| $E_{\gamma1}$-$E_{\gamma2}$ | $P_{exp}(\gamma1)$ | Spin-parity | $\delta_{exp}(\gamma1)$ | $P_{th}(\gamma1)$ |
|---|---|---|---|---|
| 858.90-814.90 | 0.26(11) | $4^+$ - $2^+$ - $0^+$ | 0.0 | 0.1667 |
| 858.90-814.90$^p$ | 0.31(10) | $4^+$ - $2^+$ - $0^+$ | $0.0^p$ | $0.1667^p$ |
| 1092.90-858.90 | 0.50(20) | $4^+$ - $4^+$ - $2^+$ | 0.54(8) | 0.269(2) |
| | | $5^-$ - $4^+$ - $2^+$ | 0.11(4) | 0.146(13) |
| | | $5^-$ - $4^+$ - $2^+$ | 5.2(12) | 0.293(18) |
| 1371.3-814.90 | 0.7(3) | $2^+$ - $2^+$ - $0^+$ | 0.15(6) | 0.452(3) |
| | | $3^-$ - $2^+$ - $0^+$ | 0.35(5) | 0.279(26) |
| | | $3^-$ - $2^+$ - $0^+$ | 1.7(2) | 0.520(5) |

or $6^+ - 4^+ - 2^+$ solution. We put tentative spin-parity6, $(7^-)$ for the 3787.4-keV level.

Tentative spin-parity assignments to higher-energy states were suggested based on the observed decays and the yrast-population argument.

As a final comment we note that the high admixture of the M2 multipolarity in the 1092.90- and 1371.3-keV transitions is an intriguing observation. An alternative, positive-parity assignment to 2186.1- and 2766.7-keV levels would change significantly the systematic picture of octupole collectivity in the region. The spin-parity of the 3787.4-keV level needs a clarification to decide if there is only a negative-parity band at medium spins [18] or also a positive- parity band as suggested in Ref. [26]. More precise multipolarity measurements for transitions in $^{92}$Sr are needed, for example a high-statistics measurement of $\gamma$ rays following neutron-induced fission of $^{233}$U.

### C. Excitations in $^{94}$Sr

The previous study of $^{94}$Sr [18] was focused on negative-parity, medium-spin levels aimed at identifying the $(h_{11/2}, g_{7/2})_{9^-}$ two-neutron configuration involving the important $h_{11/2}$ neutron level. This level, crucial for the development of nuclear deformation in the region [30–34], has not been observed directly to date [35]. In the present work, in addition to confirming the negative-parity assignments proposed in Ref. [35], which replaced earlier positive-parity assignments [36], we have searched for new, medium-spin, positive-parity states, a possible signature of a quadrupole collectivity developing in the chain of strontium isotopes [37].

Positive-parity, low-spin levels of $^{94}$Sr were reported in a measurement of $\gamma$ rays from $\beta$-decay of $^{94}$Rb [38], but some of them with incorrect parity assignments as shown in the compilation [39]. Because of the $I^\pi$=$3^-$ spin-parity of the ground of $^{94}$Rb [40], $0^+$ levels were not seen in Ref. [38]. Recent neutron-transfer-reaction study [41] reported two low-lying $0^+$ levels in $^{94}$Sr.

Excited states in $^{94}$Sr observed in this work are listed in Table VIII and shown in Fig. 5. Spin-parity assignments in Fig. 5 and Table VIII are based on the angular and directional-polarization correlations measured in this work and listed in Tables IX and X. All transitions shown in Table VIII correspond to prompt-$\gamma$ radiation following fission except the 1577.55-keV decay of the 2414.5-keV level, which is predominantly populated in $\beta$-decay of $^{94}$Rb. Many levels reported in Ref. [38] are seen in our data but not on a competitive level and except the strongly populated, 2414.5-keV level, they were not analyzed in this work. However, to assist further discussions we show in Fig. 5 several low-spin levels, drawn after Refs. [39, 41]. They are shown without decays at the right-hand side of the figure. In our data we could not see the 1043.5- and 1456.1-keV decays of the newly proposed $0^+$ levels at 1879.7 and 2292.8 keV [41]. The important new results are discussed below.

The ground-state cascade, shown to the left of Fig. 5 has been extended up to spin ($8^+$). Angular and directional-polarization correlations uniquely determine spin-parity assignments up to spin $6^+$. Spins and parities of higher-energy levels are proposed based on the observed decay branching and the yrast argument [29].

The $3^+$ spin-parity of the 2414.50-keV level was reported in Ref. [41] based on the DWBA analysis favoring positive parity, though still consistent with the negative parity, tentatively proposed in the past [38, 39]. Our search for the low-energy $3^+$ level in $^{94}$Sr was prompted by the Shell Model results reported in Ref. [18], where the experimental data was insufficient for its identification. Present results determine uniquely the $3^+$ spin-parity of the 2414.50-keV level. We note a good match of the mixing ratio, $\delta$ obtained in this work with that reported in [39]. The $\chi^2/N$ analysis of the combined angular correlations and linear polarization for the 1577.55-836.95-keV cascade is illustrated in Fig. 6, where we show $\chi^2/N$ solutions for various spin-parity hypotheses of the 2414.50-keV level (more information about this technique can be found in Sec. 4 of Ref. [23]).

The multipolarity analysis for the 710.90-(1309.05+836.95)-keV cascade indicates spin-parity $5^+$ for the 2856.9-keV level, reported as $(5)^-$ in the compilation [39]. The negative parity reported in Ref. [18] was a result of underestimating the 709.4-keV component admixture in the 711-keV complex line. The present high-statistics data allowed a better fit to the doublet. The positive parity of the 2856.9-keV level is supported by the multipolarity analysis for the 253.00-677.70-keV cascade, indicating a pure stretched E1 multipolarity of the 253.00-keV decay to the $4^-$ level at 2604.1 keV (see below). Tentative spin-parity of 4034.6- and 4952.9-keV levels are based on decay branching and the yrast- population argument [29].

Levels at 2414.50, 2649.8, 2856.9, 3705.8, 4034.6 and 4952.9 keV, shown in the middle of Fig. 5 can be ar-

TABLE VIII: Experimental properties of excited levels in $^{94}$Sr populated in neutron-induced fission of $^{235}$U (except the 2414.50-keV level - see text). New information is marked by asterisks. Explanation of other symbols as in Table II.

| $E_i$ (keV) | $I_i^\pi$ | $E_\gamma$ (keV) | $I_\gamma$ (rel.) | $E_f$ (keV) | $I_f^\pi$ |
|---|---|---|---|---|---|
| 836.95(5) | $2^+$ | 836.95(5) | | 0.0 | $0^+$ |
| 1926.40(8) | $3^-$ | 1089.45(5) | | 836.95 | $2^+$ |
| 2146.00(8) | $4^+$ | 1309.05(5) | | 836.95 | $2^+$ |
| 2414.50(8) | $3^+$ * | 1577.55(5) | | 836.95 | $2^+$ |
| 2604.1(1) | $4^-$ * | 189.5(2) * | 1.2(4) | 2414.50 | $3^+$ |
| | | 458.2(1) | 24(2) | 2146.00 | $4^+$ |
| | | 677.70(5) | 100(3) | 1926.40 | $3^-$ |
| | | 1766.7(3) | 1.4(5) | 836.95 | $2^+$ |
| 2649.8(1) | $4^+$ * | 235.5(3) * | 2(1) | 2414.50 | $3^+$ |
| | | 503.9(1) | 100(3) | 2146.00 | $4^+$ |
| | | 723.3(2) | 30(5) | 1926.40 | $3^-$ |
| | | 1812.7(1) | 85(5) | 836.95 | $2^+$ |
| 2739.4(2) | $4^{(-)}$ * | 813.0(1) | 100(5) | 1926.40 | $3^-$ |
| | | 1902.3(2) | 6(1) | 836.95 | $2^+$ |
| 2856.9(1) | $5^+$ * | 117.4(1) | 27(2) | 2739.4 | $4^{(-)}$ |
| | | 207.20(5) | 28(2) | 2649.8 | $4^+$ |
| | | 253.00(5) | 100(3) | 2604.1 | $4^-$ |
| | | 710.90(5) | 88(3) | 2146.00 | $4^+$ |
| 2972.0(1) | $5^-$ * | 826.00(5) | 100(8) | 2146.00 | $4^+$ |
| | | 1045.60(5) | 82(6) | 1926.40 | $3^-$ |
| 3155.9(1) | $6^+$ | 184.1(1) | 25(2) | 2972.0 | $5^-$ |
| | | 299.00(5) | 66(3) | 2856.9 | $5^+$ |
| | | 1009.90(5) | 100(3) | 2146.00 | $4^+$ |
| 3310.6(1) | $5^-$ * | 661.0(2) | 75(5) | 2649.8 | $4^+$ |
| | | 1384.3(1) | 100(5) | 1926.40 | $3^-$ |
| 3705.8(2) | $6^{(+)}$ | 849.0(3) | 15(5) | 2856.9 | $5^+$ |
| | | 1559.8(1) | 100(3) | 2146.00 | $4^+$ |
| 3793.2(1) | $6^-$ * | 482.6(1) | 55(5) | 3310.6 | $5^-$ |
| | | 637.3(1) | 65(5) | 3155.9 | $6^+$ |
| | | 1189.1(1) | 100(3) | 2604.1 | $4^-$ |
| 3923.3(1) | $7^-$ * | 130.20(5) | 35(2) | 3793.2 | $6^-$ |
| | | 217.4(2) | 2(1) | 3705.8 | $6^{(+)}$ |
| | | 612.8(2) | 7(1) | 3310.6 | $5^-$ |
| | | 767.35(5) | 100(3) | 3155.9 | $6^+$ |
| | | 951.15(5) | 26(2) | 2972.0 | $5^-$ |
| | | 1066.5(3) | 9(2) | 2856.9 | $5^+$ |
| 3952.2(3) * | $(6^+)$ | 1806.2(2) * | | 2146.00 | $4^+$ |
| 4034.6(2) | $(7^+)$ * | 878.6(1) | 100(8) | 3155.9 | $6^+$ |
| | | 1177.9(3) | 45(5) | 2856.9 | $5^+$ |
| 4360.3(3) * | $(8^+)$ * | 1204.4(2) * | | 3155.9 | $6^+$ |
| 4383.2(2) | $(8^-)$ | 459.70(5) | | 3923.3 | $7^-$ |
| 4435.5(3) * | $(7^+)$ | 483.3(2) * | | 3952.2 | $(6^+)$ |
| 4632.9(2) | $(8^-)$ | 249.8(2) | 25(2) | 4383.2 | $(8^-)$ |
| | | 598.20(5) | 40(5) | 4034.6 | $(7^+)$ |
| | | 709.4(1) | 100(3) | 3923.3 | $7^-$ |
| 4858.9(2) | $(9^-)$ | 226.1(1) | 100(5) | 4632.9 | $(8^-)$ |
| | | 475.6(1) | 85(5) | 4383.2 | $(8^-)$ |
| | | 935.3(1) | 30(5) | 3923.3 | $7^-$ |
| 4892.5(4) * | $(8^+)$ | 457.0(2) * | | 4435.5 | $(7^+)$ |
| 4952.9(3) * | $(8^+)$ | 1000.8(2) * | 100(15) | 3952.2 | $(6^+)$ |
| | | 1247.1(1) * | 30(10) | 3705.8 | $6^{(+)}$ |
| 5741.3(3) | $(10,11^-)$ | 882.4(1) | | 4858.9 | $(9^-)$ |
| 5815.0(3) * | $(9,10^+)$ | 862.1(2) * | | 4952.9 | $(8^+)$ |
| | | 922.6(3) * | | 4892.5 | $(8^+)$ |
| 6920.7(4) * | $(12,13^-)$ | 1179.4(2)* | | 5741.3 | $(10,11^-)$ |
| 7262.4(5) * | $(14,15^-)$ | 341.7(2) * | | 6920.7 | $(12,13^-)$ |

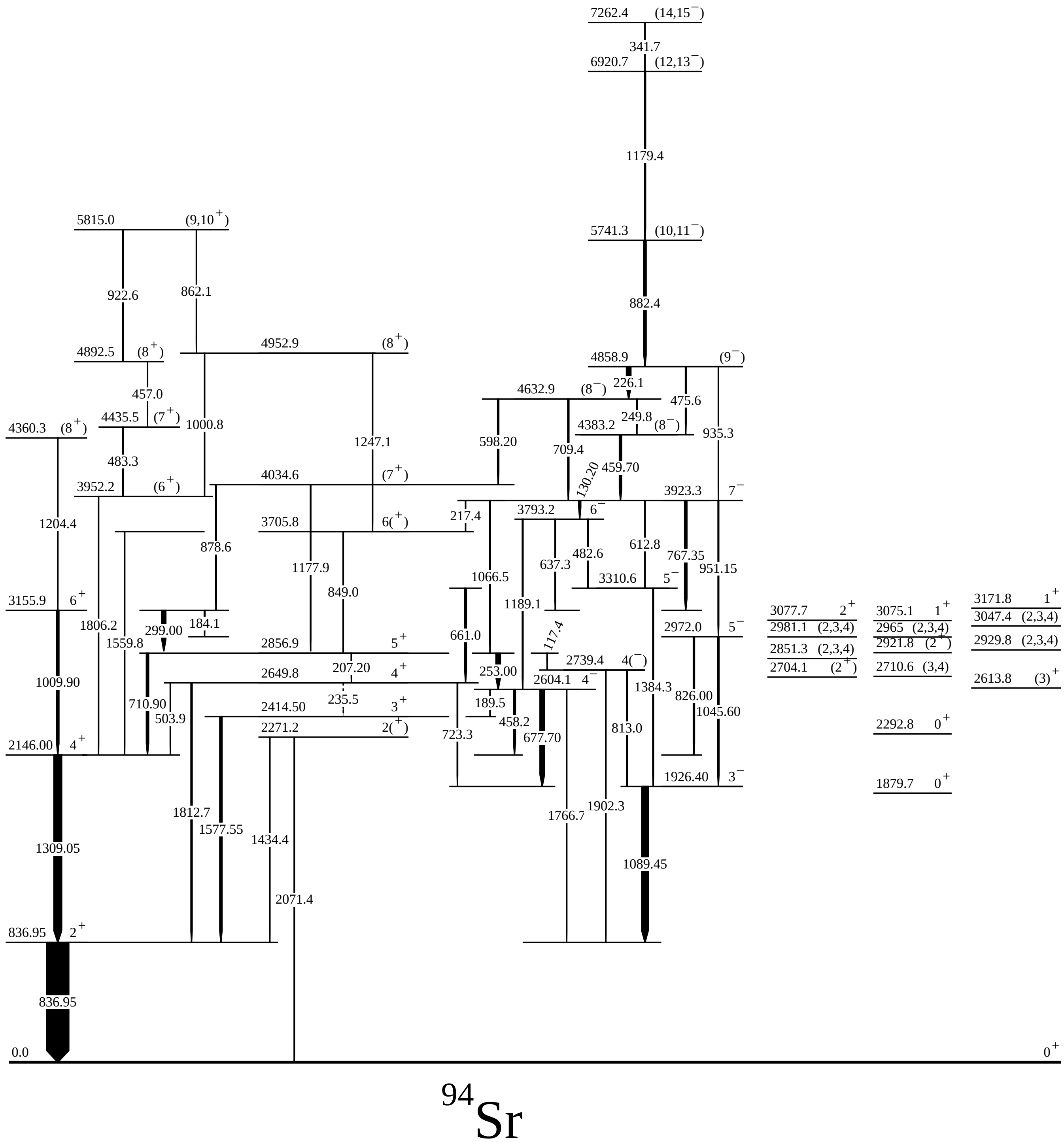


FIG. 5: Partial level scheme of $^{94}$Sr obtained in this work in a measurement of $\gamma$ rays following neutron-induced fission of $^{235}$U. Levels without decays, shown to the right, and the 2271.2-keV level are drawn after Refs. [39, 41] to assist further discussions.

ranged into a band because of linking transitions. Here we included also the 2271.2-keV level populated in $\beta$ decay [38], with a tentative ($2^+$) spin-parity [39]. Spin I=2 is supported by the fact that, unlike the nearby $3^+$ at 2414.50 keV, the 2271.2-keV level is not populated directly in fission.

The new structure above the 2271.2-keV level is a candidate for a $\gamma$ band in $^{94}$Sr with a possible $2^+_2$ head

TABLE IX: Angular correlation coefficients for $\gamma-\gamma$ cascades in $^{94}$Sr populated in neutron-induced fission of $^{235}$U. Label "sum" denotes summed correlations with all quadrupole transitions below the $E_{\gamma 1}$.

| $E_{\gamma 1}$-$E_{\gamma 2}$ cascade | $A_2/A_0$ exp. | $A_4/A_0$ exp. | Spins in cascade | $\delta_{exp}(E_{\gamma 1})$ |
|---|---|---|---|---|
| 253.00-677.70 | 0.127(10) | -0.010(23) | 5 - 4 - 3 | 0.02(1) |
| 1089.45-836.95 | -0.068(10) | -0.020(22) | 3 - 2 - 0 | 0.005(12) |
| 1309.05-836.95 | 0.104(8) | -0.022(18) | 4 - 2 - 0 | |
| 1577.55-836.95 | -0.070(9) | -0.018(18) | 3 - 2 - 0 | 0.002(12) |
| 1812.65-836.95 | 0.093(26) | 0.020(60) | 4 - 2 - 0 | |
| 503.9-sum | 0.190(23) | 0.030(56) | 4 - 4 - 2 | 0.02(8) or -0.97(15) |
| 1009.90-sum | 0.111(12) | -0.021(27) | 6 - 4 - 2 | |
| 767.35-1009.90 | -0.083(15) | 0.005(34) | 7 - 6 - 4 | -0.017(24) |
| 677.70-1089.45 | 0.313(10) | 0.004(24) | 4 - 3 - 2 | -1.5(3) or -0.9(2) |
| 813.0-1089.45 | 0.041(20) | -0.041(43) | 4 - 3 - 2 | 0.02(4) or 7.7(19) |
| 1384.3-1089.45 | -0.049(37) | 0.11(8) | 5 - 3 - 2 | |
| 710.90-1309.05 | -0.224(13) | -0.013(26) | 5 - 4 - 2 | -0.23(3) or -6.8(9) |
| 826.00-1309.05 | -0.065(23) | -0.011(47) | 5 - 4 - 2 | 0.01(4) |

TABLE X: Experimental, $P_{exp}(\gamma_1)$ and theoretical, $P_{th}(\gamma_1)$ values of linear polarization for the $\gamma_1$ (upper) transition in a $\gamma_1-\gamma_2$ cascade of $^{94}$Sr, populated in neutron-induced fission of $^{235}$U, as obtained in this work. The correlating $\gamma_2$ transitions of 836.95 keV and 1309.05 keV are assumed to be stretched, E2 with $\delta$=0.

| $E_{\gamma 1}$-$E_{\gamma 2}$ | $P_{exp}(\gamma 1)$ | Spin-parity | $\delta_{exp}(\gamma 1)$ | $P_{th}(\gamma 1)$ |
|---|---|---|---|---|
| 1089.45-836.95 | 0.08(3) | $3^-$ - $2^+$ - $0^+$ | 0.005(12) | 0.106(5) |
| 1309.05-836.95 | 0.175(45) | $4^+$ - $2^+$ - $0^+$ | 0.0 | 0.1667 |
| 1577.55-836.95 | -0.26(9) | $3^+$ - $2^+$ - $0^+$ | 0.002(16) | -0.104(7) |
| 1812.7-836.95 | 0.57(24) | $4^+$ - $2^+$ - $0^+$ | 0.0 | 0.1667 |
| 503.9-1309.05 | -0.01(9) | $4^+$ - $4^+$ - $2^+$ | 0.02(7) | 0.329() |
| | | | -0.97(15) | 0.035(20) |
| 710.90-1309.05 | -0.34(8) | $5^+$ - $4^+$ - $2^+$ | -0.23(3) | -0.035(7) |
| | | | -6.8(9) | -0.162(8) |
| 1009.90-1309.05 | 0.11(6) | $6^+$ - $4^+$ - $2^+$ | -0.23(3) | 0.1667 |

at 2271.2 keV. The link to the head is not observed most likely because of the unfavoured branching from the 2414.50- and 2649.8-keV levels. However, the missing E2 link between the 2856.9- and 2414.50-keV levels and the high intensity of the 253.00-keV, E1 decays from the 2856.9-keV level are puzzling. In Ref. [41] a single-particle character of the $3^+$ level at 2414.50-keV was considered.

Above the 1926.40-keV level one observes a cascade consisting of negative-parity level. The $3^-$ spin-parity of the 1926.40-keV level is uniquely determined by multipolarity analysis for the 1089.45-836.95-keV cascade. The analysis for the 677.70-1089.45-keV cascade uniquely de-

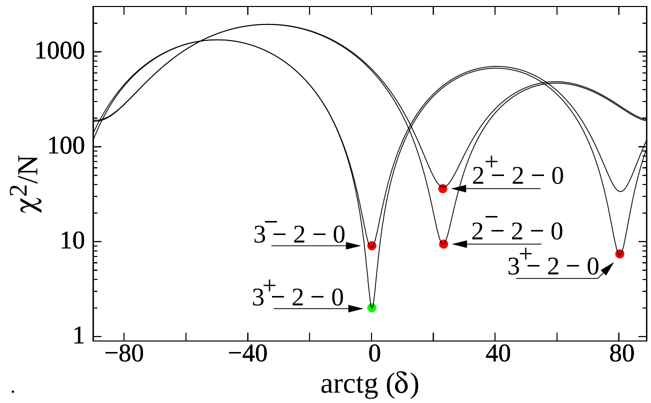


FIG. 6: The combined angular and directional-polarization correlation analysis of transition mutipolarities in the 1577.55-836.95-keV cascade in $^{94}$Sr, populated in the neutron-induced fission of $^{235}$U. See text for more explanations.

termines spin-parity $4^-$ of the 2604.1-keV level. This agrees with the stretched E1 feeding from the $5^+$ level at 2856.9-keV. The multipolarity analysis for the 826.0-1309.05-keV cascade indicates spin-parity $5^-$ for the 2972.0-keV level and the analysis for the 767.35-1009.90-keV cascades indicates spin-parity $7^-$ for the 3923.3-keV level. Spin-parity assignments to levels at higher energies are proposed based on the observed decay branching and the yrast-population argument [29].

A clear population in fission of $^{235}$U of the 2613.8- and 2710.6-keV levels and its lack for the 2704.1-keV level suggests spin of the 2613.8- and 2710.6-keV levesl higher than ths spin of the 2704.1-keV level. Taking into account the data reported in Refs. [39, 41] we thus propose spin I=$(3)^+$ for the 2613.8-keV level, spin I=(3,4) for the 2710.6-keV and spin I=$(2^+)$ for the 2704.1-keV level.

### D. Excitations in $^{96}$Sr

Low-spin excitations of $^{96}$Sr were studied before in a measurement of $\gamma$ rays from $\beta$-decay of the $2^+$ ground state of $^{96}$Rb [42], in Coulomb excitations [43, 44], in transfer reactions [45, 46] and in timing measurements of levels populated in neutron-induced fission of $^{235}$U [37]. Medium-spin levels of $^{96}$Sr were reported before in a measurement of $\gamma$ rays following spontaneous fission of $^{248}$Cm [18, 33, 47–49] and in $\alpha$-induced fusion-fission of $^{238}$U [50]. The present study of $^{96}$Sr, based on a neutron-induced fission of $^{235}$U and spontaneous fission of $^{252}$Cf, updates and extends previous data.

Excited levels in $^{96}$Sr observed in this work are listed in Table XI and shown in Fig. 7. All transitions shown in Table XI, except the 649.0-keV decay from the $0_3^+$ level at 1464.0 keV, are observed as prompt- $\gamma$ rays following fission. To assist further discussions we show to the right-hand side of Fig. 7 several low-spin levels, drawn after Refs. [46, 51]. These levels are populated predominantly in $\beta^-$ decay of $^{96}$Rb and are not part of any medium-spin cascades. However, some of them are weakly populated in prompt-$\gamma$ fission, the observation which will help verifying their spin assignments.

Spin-parity assignments to levels in $^{96}$Sr shown in Table XI and Fig. 7 are based on angular and directional-polarization correlations measured in this work and listed in Tables XII and XIII, respectively. New results obtained in this work are marked with asterisks in Table XI.

The most important new result in $^{96}$Sr is the observation of the 277.7-keV, E2 in-band decay of the $2^+$ level at 1507.0 keV to the $0^+$ level at 1229.5 keV, completing the deformed band based on the second $0^+$ level in $^{96}$Sr. The observed branching for the 277.7-keV transition, which is an average value obtained from the $^{252}$Cf and $^{235}$U fission data, together with the 6 ps upper limit on the half-life of the 1507.0-keV level, provides a lower limit of B(E2)≥38(8) W.u. on the rate of the 277.7-keV transition, confirming the deformed band of moderate collectivity on top of the 1229.5-keV, $0^+_2$ level [33].

Another important comment concerns the 40(8) ns half-life of the 3524.7-keV isomer, reported in Ref. [33]. The present work does not confirm this value. From the delayed-time spectrum for the 398.55-keV transition, observed in the $^{252}$Cf fission data, we deduce a half-life, $T_{1/2}$=10(5) ns for this isomer. Further work is needed to explain this discrepancy.

Spin-parity assignments to the 815.00- and 1792.80-keV levels are adopted after the compilation [51]. Unique spin-parity assignments to the 2466.8-, 3126.1- and 3524.7-keV levels are determined based on the angular and directional-polarization correlations listed in Tables XII and XIII, confirming assignments reported in our previous works [18, 33]. Analogously, unique spin-parity assignments are determined for the 1507.0-, 1628.6- and 1975.9-keV levels confirming assignments reported in Refs. [33, 51].

The multipolarity analysis for the 993.2-977.80-keV cascade indicates spin-parity $6^+$ for the 2786.0-keV level. Subsequent analysis for the 542.90-sum cascade (see Table XII) indicates spin I=7 for the 3328.9-keV level. The $I^\pi=9^-$ spin parity of the 3524.7-keV isomer imposes the stretched, E2 character on its 195.6-keV decay, indicating a negative parity for the 3328.9-keV level.

The analysis for the 1037.6-815.00-keV cascade shows that the 1037.6-keV transition is not a stretched quadrupole and puts I<4 limit on the spin of the 1852.6-keV level. On the other hand, the prompt 595.5-881.2-keV cascade from the 3328.9-keV level gives I>2. The resulting spin I=3 of the 1852.6-keV level indicates spin I=5 for the 2733.6-keV level and a negative parity for both levels.

The analysis for the 1305.10-815.00-keV cascade indicates spin-parity $I^\pi=4^+$ for the 2120.1-keV level.

Spins and parities of other levels in cascades are proposed based on the yrast-population argument [29] and decay branching. In particular, a tentative I=6($^+$) spin-

TABLE XI: Experimental properties of excited levels in $^{96}$Sr populated in neutron-induced fission of $^{235}$U (except the 1464.0-keV level - see text). New information is marked by asterisks. Explanation of other symbols as in Table II.

| $E_i$ (keV) | $I_i^\pi$ | $E_\gamma$ (keV) | $I_\gamma$ (rel.) | $E_f$ (keV) | $I_f^\pi$ |
|---|---|---|---|---|---|
| 815.00(5) | $2^+$ | 815.00(5) | | 0.0 | $0^+$ |
| 1229.5(2) | $0^+$ | 414.5(1) | | 815.00 | $2^+$ |
| 1464.0(5) | $0^+$ | 649.0(5) | | 815.00 | $2^+$ |
| 1507.0(1) | $2^+$ | 277.7(2) * | 2.8(5) * | 1229.5 | $0^+$ |
| | | 692.00(5) | 100(3) | 815.00 | $2^+$ |
| | | 1506.95(5) | 53(2) | 0.0 | $0^+$ |
| 1628.6(1) | $2^+$ * | 399.0(2) | 15(3) | 1229.5 | $0^+$ |
| | | 813.6(1) | 100(8) | 815.00 | $2^+$ |
| | | 1628.9(3) | 5(3) | 0.0 | $0^+$ |
| 1792.80(8) | $4^+$ | 977.80(5) | | 815.00 | $2^+$ |
| 1852.6(2) | $3^-$ * | 345.5(5) | 70(30) | 1507.0 | $2^+$ |
| | | 1037.6(1) | 100(20) | 815.00 | $2^+$ |
| 1975.9(1) | $4^+$ * | 347.3(1) | 18(1) | 1628.6 | $2^+$ |
| | | 468.9(1) | 100(3) | 1507.0 | $2^+$ |
| | | 1160.8(1) | 54(2) | 815.00 | $2^+$ |
| 2120.1(1) | $4^+$ * | 327.3(1) | 11(3) | 1792.80 | $4^+$ |
| | | 1305.10(5) | 100(5) | 815.00 | $2^+$ |
| 2466.8(1) | $6^+$ * | 491.00(5) | 82(3) | 1975.9 | $4^+$ |
| | | 674.00(5) | 100(3) | 1792.8 | $4^+$ |
| 2481.0(2) | $(5^+)$ * | 361.0(1) | 97(14) | 2120.1 | $4^+$ |
| | | 688.1(1) | 100(12) | 1792.80 | $4^+$ |
| 2493.0(3) | $(0^+)$ | 1678.0(2) | | 815.00 | $2^+$ |
| 2733.6(2) * | $5^-$ * | 881.2(2) * | 30(15) | 1852.6 | $3^-$ |
| | | 940.7(1) | 100(20) | 1792.80 | $4^+$ |
| 2786.0(1) | $6^+$ * | 810.3(1) | 50(3) | 1975.9 | $4^+$ |
| | | 993.20(5) | 100(3) | 1792.80 | $4^+$ |
| 2899.8(2) | $(6^+)$* | 779.6(1) | 100(20) | 2120.1 | $4^+$ |
| | | 1107.0(1) | 66(12) | 1792.80 | $4^+$ |
| 3010.6(3) | (5) | 1217.8(2) | | 1792.80 | $4^+$ |
| 3126.1(2) | $8^+$ * | 659.30(5) | | 2466.8 | $6^+$ |
| 3239.3(3) | $(7^+)$ * | 339.6(2) | 30(10) | 2899.8 | $(6^+)$ |
| | | 758.3(1) | 100(20) | 2481.0 | $(5^+)$ |
| 3328.9(2) | $7^-$ | 542.90(5) | 100(6) | 2786.0 | $6^+$ |
| | | 595.5(2) | 20(4) | 2733.6 | $5^-$ |
| | | 862.1(1) | 19(5) | 2466.8 | $6^+$ |
| 3524.7(3) | $9^-$ | 195.6(1) | 21(4) | 3328.9 | $7^-$ |
| | | 398.55(5) | 100(5) | 3126.1 | $8^+$ |
| 3605.4(2) | $(6^+)$ | 594.6(3) | 43(15) | 3010.6 | (5) |
| | | 1138.7(1) | 100(12) | 2466.8 | $6^+$ |
| | | 1812.4(2) | 52(14) | 1792.80 | $4^+$ |
| 3708.5(3) * | $(8^+)$ | 922.5(2) * | | 2786.0 | $6^+$ |
| 3852.5(3) | $(7^+)$ | 247.1(1) | | 3605.4 | $(6^+)$ |
| 3887.3(3) | $(10^+)$ | 761.2(1) | | 3126.1 | $8^+$ |
| 4132.2(4) | $(8^+)$ | 279.7(1) | | 3852.5 | $(7^+)$ |
| 4133.4(3) | $(8,9^-)$ | 804.5(1) | | 3328.9 | $7^-$ |
| 4331.1(4) | $(10,11^-)$ | 806.4(1) | | 3524.7 | $9^-$ |
| 4444.2(5) | (9+) | 312.0(1) | | 4132.2 | $(8^+)$ |
| 4725.6(4) | $(12^+)$ | 838.3(1) | | 3887.3 | $(10^+)$ |
| 4787.0(5) | $(10^+)$ | 342.8(2) | | 4444.2 | $(9^+)$ |
| 5161.0(7) * | $(11^+)$ | 374.0(5) * | | 4787.0 | $(10^+)$ |
| 5390.2(5) * | (11,12) | 1059.1(2)* | | 4331.1 | $(10,11^-)$ |
| 5752.5(6) * | $(12,13^-)$ | 1421.4(1) * | | 4331.1 | $(10,11^-)$ |
| 6007.8(6) * | (13,14) | 255.3(2) * | | 5752.5 | $(12,13^-)$ |
| | | 618.1(3) * | | 5390.2 | (11,12) |
| 6213.8(7) * | (14,15) | 206.0(2) * | | 6007.8 | (13,14) |

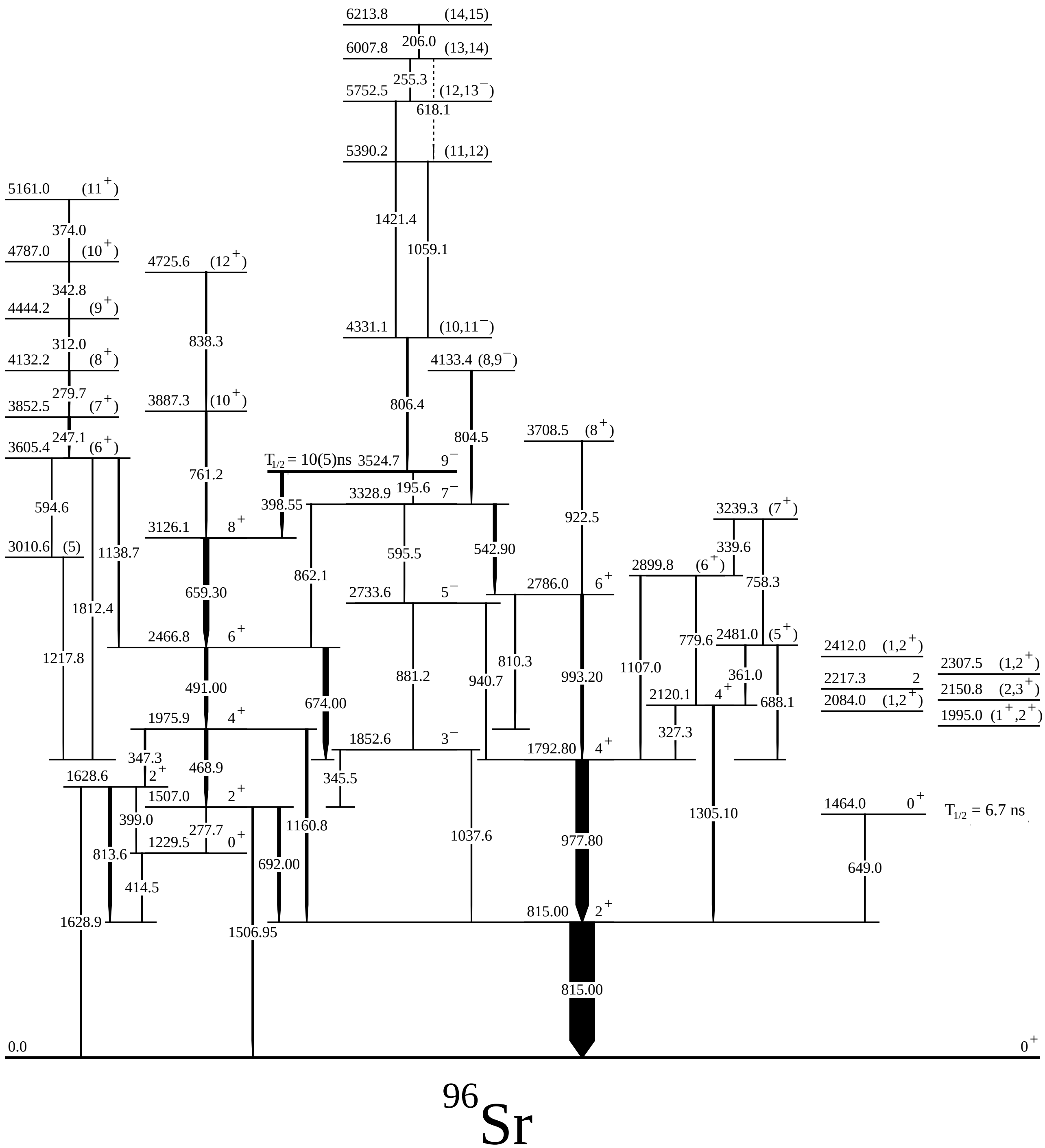


FIG. 7: Partial level scheme of $^{96}$Sr obtained in this work from measurements of $\gamma$ rays following spontaneous fission $^{252}$Cf and neutron-induced fission of $^{235}$U. Levels at the right-hand side (shown without their decays ) are drawn after Refs. [46, 51].

parity for the 3605.4-keV level is suggested by the 1812.4-keV decay to the $4^+$ level at 1792.80 keV and the yrast population argument applied to the 3605.4-keV level.

A clear population in fission of $^{235}$U of the 2150.8-keV suggests spin higher than I=1 for this level. Taking into account the data reported in Refs. [46, 51] we thus propose spin I=(2,$3^+$) for the 2150.8-keV level. The levels at 2493.0 keV and 2704.0 keV are possible candidates for $0^+$ excitations in $^{96}$Sr. This is supported by angular correlations for the 1678.0-815.00-keV and 1889.0-815.00-

TABLE XII: Angular correlation coefficients for $\gamma-\gamma$ cascades in $^{96}$Sr populated in neutron-induced fission of $^{235}$U. Label "sum" denotes summed correlations with all quadrupole transitions below the $E_{\gamma1}$. Superscript "a" indicates mixed transition, if not $\gamma_1$.

| $E_{\gamma1}$-$E_{\gamma2}$ cascade | $A_2/A_0$ exp. | $A_4/A_0$ exp. | Spins in cascade | $\delta_{exp}(E_{\gamma1})$ |
|---|---|---|---|---|
| 398.55 - sum | -0.125(10) | -0.008(22) | 9 - 8 - 6 | -0.09(2) |
| 414.5 - 815.00 | 0.33(9) | 0.67(18) | 0 - 2 - 0 | |
| 468.9 - 692.00$^a$ | 0.128(17) | -0.060(37) | 4 - 2 - 2 | 0.77(15) or 3.4(11) |
| 491.0 - 468.9 | 0.096(14) | 0.003(31) | 6 - 4 - 2 | |
| 542.90 - sum | -0.062(25) | -0.048(45) | 7 - 6 - 4 | 0.02(4) |
| 649.0 - 815.00 | 0.36(15) | 0.80(32) | 0 - 2 - 0 | |
| 659.30 - 674.00 | 0.113(15) | -0.003(33) | 8 - 6 - 4 | |
| 659.30 - 491.00 | 0.098(14) | -0.049(29) | 8 - 6 - 4 | |
| 674.00 - sum | 0.097(10) | -0.018(21) | 6 - 4 - 2 | |
| 692.00 - 815.00 | -0.246(17) | 0.173(34) | 2 - 2 - 0 | 0.87(7) |
| 813.6 - 815.00 | -0.015(18) | 0.058(39) | 2 - 2 - 0 | 0.35(3) |
| 993.20 - sum | 0.117(19) | -0.019(43) | 6 - 4 - 2 | |
| 1037.6 - 815.00 | -0.036(28) | 0.048(55) | 3 - 2 - 0 | 0.05(4) |
| 1160.8 - 815.00 | 0.095(21) | -0.022(44) | 4 - 2 - 0 | |
| 1305.10 - 815.00 | 0.105(25) | -0.068(54) | 4 - 2 - 0 | |

TABLE XIII: Measured, $P_{exp}(\gamma_1)$ and calculated, $P_{th}(\gamma_1)$ values of linear polarization for the $\gamma_1$ transition in a $\gamma_1-\gamma_2$ cascade of $^{96}$Sr, as obtained in this work. The correlating $\gamma_2$ of 815.00 keV is assumed to be a stretched, E2 transition with $\delta$=0. Label "sum" denotes summed correlations with all quadrupole transitions below the $E_{\gamma1}$.

| $E_{\gamma1}$-$E_{\gamma2}$ | $P_{exp}(\gamma1)$ | Spin-parity | $\delta_{exp}(\gamma1)$ | $P_{th}(\gamma1)$ |
|---|---|---|---|---|
| 398.55 - sum | 0.11(6) | $9^-$ - $8^+$ - $6^+$ | -0.09(2) | 0.075(7) |
| 414.5 - 815.00 | 1.2(5) | $0^+$ - $2^+$ - $0^+$ | 0.0 | 1.0000 |
| 659.30 - sum | 0.19(6) | $8^+$ - $6^+$ - $4^+$ | 0.0 | 0.1667 |
| 674.00 - sum | 0.22(7) | $6^+$ - $4^+$ - $2^+$ | 0.0 | 0.1667 |
| 977.80 - 815.00 | 0.16(4) | $4^+$ - $2^+$ - $0^+$ | 0.0 | 0.1667 |
| 993.2 - 977.80 | 0.45(38) | $6^+$ - $4^+$ - $2^+$ | 0.0 | 0.1667 |
| 1160.8 - 815.00 | 0.16(8) | $4^+$ - $2^+$ - $0^+$ | 0.0 | 0.1667 |
| 1305.10 - 815.00 | 0.40(28) | $4^+$ - $2^+$ - $0^+$ | 0.0 | 0.1667 |

keV cascades showing large $A_4/A_0$ values and the lack of population on these levels in fission of $^{235}$U.

## III. DISCUSSION

For the evolution of nuclear deformation in the A≈100 region the crucial issue is the "early" population of the neutron $g_{7/2}$ and the proton $g_{9/2}$ shells. The population of the proton $g_{9/2}$ orbital seem to be particularly sudden, giving rise to a strong deformation already at Z=38. Various explanations were proposed in the past. Federman and Pittel [52] proposed the population of $g_{9/2}$ protons via the monopole interaction with the $g_{7/2}$ neutrons - the Spin-Orbit-Partner (SOP) mechanism. However, this does not explain the early population of the $g_{7/2}$ neutrons. More recently an analogous, "self-reinforcing" [53] mechanism was proposed, driven by the monopole tensor interaction between the two orbitals [54], but again, the early population of the $g_{7/2}$ neutrons was not addressed.

We note, that in the Nilsson scheme, there are strongly upsloping $3/2^-$[301], $5/2^-$[303] and $1/2^-$[301] proton orbitals, crossing the down-slopping, $1/2^+$[440], $3/2^+$[431] and $5/2^+$[422] orbitals of the $g_{9/2}$ parentage. With the increasing deformation the upsloping orbitals deliver six extra protons to the Fermi level, which populate the $g_{9/2}$ shell helping to create deformed minimum in the nuclear potential. This action may begin already in Se isotopes at Z=34 (see e.g. Fig. 8 in Ref. [55]). Indeed, in Br isotopes the $g_{9/2}$ proton excitation is observed at about 1.5 MeV [17, 56], an energy lower than expected from the scheme of spherical shells.

Less evident is the early population of the neutron $g_{7/2}$ shell and its role in the shape coexistence in the region. As noted in Ref. [57] this orbital is populated already at N=52. A pair of neutrons can be promoted across the N=50 gap from the $g_{9/2}$ to the $g_{7/2}$ shell creating $0^+$ excited levels at relatively low excitation, analogous to $0^+$ intruder states in Sn isotopes created by promoting a pair of protons across the Z=50 line [58]. The SOP mechanism and the action of the $9/2^+$[404] extruder [59, 60], which promotes two extra neutrons to the Fermi surface (see e.g. Fig. 9 in Ref. [55]) further increase the population of the $g_{7/2}$ shell, resulting in lowering such $0^+$ energies with the growing neutron number.

Below we discuss these ideas in more detail, assisted by the Large-Scale Shell-Model (LSSM) calculations performed using the natural valence space outside the $^{78}$Ni core, comprising the $\pi 1f_{5/2}, 2p_{3/2}, 2p_{1/2}, 1g_{9/2}$ and $\nu 2d_{5/2}, 3s_{1/2}, 2d_{3/2}, 1g_{7/2}, 1h_{11/2}$ orbitals. The model space and interaction were previously employed in the studies of a large number of nuclei in the region, see e.g. [16, 18, 56, 57, 61–64]. In particular it has proven successful in the description of the zirconium isotopic chain below $N = 60$ [61]. It thus seems particularly suited for investigating the structure of low energy excitations in Sr isotopes. As can be anticipated from this previous study [61], the strongly deformed, collective states at low energy may not be fully accounted for in the present model. However, we do not expect such states to appear at $N < 58$. The calculations were performed using the Strasbourg shell-model codes ANTOINE and NATHAN. The Sr isotopes with $N \geq 56$ pose a challenge to standard diagonalization techniques within this model space. We performed unrestricted calculations for $N = 50-54$ while 8p-8h excitations were allowed in $^{94}Sr_{56}$ and in $^{96}Sr_{58}$. Only a few lowest levels were computed in $^{96}$Sr due to the numerical complexity. The details of these calculations and an extended discussion of the theoretical results will be presented in Ref. [65].

### A. General properties of Sr isotopes

Excitation schemes of $^{90-96}$Sr, shown in Figs. 3, 4, 5 and 7 show an increase of collectivity with the growing neutron number, which is reflected in the decreasing excitation energies of low-spin levels.

The $^{90}$Sr nucleus displays features characteristic of a spherical system with the $R_{42}= E_{exc}(4^+_1)/E_{exc}(2^+_1)$ ratio of 1.99. Except the ground-state cascade no other structure is formed below 4 MeV. Two cascades, of probable s.p. nature are populated above this energy in HI-induced reaction [26].

In $^{92}$Sr the $R_{42}$=2.05 ratio is similar but there is a significant lowering of non-yrast excitations. The only "band" is observed on top of the $3^-$ octupole excitation, in accord with observations from other regions that octupole collectivity develops early outside closed shells.

In the $^{94}$Sr nucleus the $R_{42}$=2.56 ratio suggests its transitional character. This is supported by lower energies of negative-parity levels and the appearance of a $\gamma$-like band, another collectivity showing early outside closed shells.

Finally, in $^{96}$Sr a well developed rotational band, based on the $0^+_2$ level is seen. This bands has the ratio $R_{42}$=2.69 while the $R_{42}$=2.20 ratio in the ground-state cascade is lower than in $^{94}$Sr. We also note that the negative-parity band here is developed less than in $^{94}$Sr.

Summarizing, up to N=58 the collectivity in Sr isotopes increases slowly with the growing neutron number. This increase is seen in excited configurations while ground states remains spherical, as can be judged from their quadrupole moments [66].

Figure 8 shows low-energy $0^+_2$ (red circles), $2^+$ (blue open symbols), $3^-$ (green symbols) and $4^+$ (blue filled symbols) excitation energies in Sr (circles) and Zr (squares) isotopes. Above N=50, excitation energies drop quickly with the increasing neutron number but at N=56 all positive-parity levels increase significantly in energy, due to the $d_{5/2}$ neutron shell closure. The $2^+_1$ level, with nearly constant energy from N=52 to N=58 is a notable exception, which will be discussed below. One also notes a deviation of the $2^+_2$ level in $^{94}$Sr from the general trend, with the energy of the $2^+_3$ level closer to the expected position of the $2^+_2$ level. Above N=58 there is a spectacular lowering of all the levels. This suggests another mechanism of excitation there, as discussed in Ref. [1]. In contrast, negative-parity levels, which are probably due to octupole correlations, do not show such strong variations and, to date, are not known above N=58.

In the following sections we discuss various excitation modes, which may contribute to the development of collectivity seen in Fig. 8. Special attention will be devoted to $0^+$ excitations, which play an important role in quantum phase transitions (QPT) and shape coexistence phenomena in the region [67, 68]. The experimental results are compared to the LSSM calculations to learn more about the microscopic structure of Sr isotopes.

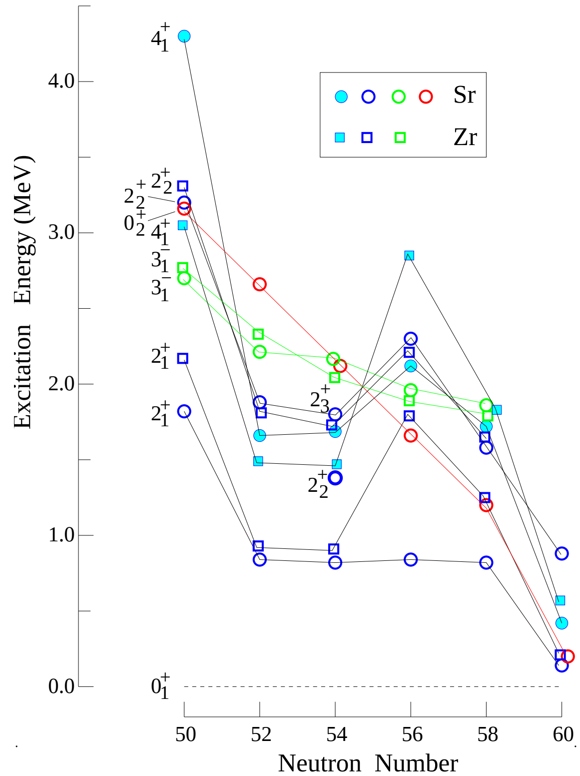


FIG. 8: Excitation energies of low-spin levels in Sr and Zr isotopes. The data are taken from the present work and from the ENSDF base [4]. See text for more comments.

### B. $0^+$ excitations

Figure 9 shows excitation energies of $0^+_2$ and $0^+_3$ levels in Sr isotopes in the neutron range 50≥N≥62. Data points corresponding to deformed $0^+$ levels are represented by filled circles. To help the discussion we included energies of $2^+_1$ excitations (empty square symbols).

Energies of $0^+_2$ levels decrease from N=50 to N=58 and then drop suddenly at N=60. The $0^+_3$ levels follow closely the trend of $0^+_2$ levels. This suggests that the $0^+_3$ levels interact weakly with $0^+_2$ levels not showing any clear "repulsion pattern ", thus not supporting strong mixing claimed in Ref. [41]. The comparison with the trend of $2^+_1$ levels suggests that the $0^+_2$ levels are rather not double-phonon excitations. They are also not due to $\beta$ vibrations, which are not expected in nuclei with spherical ground states (N≤58), while the $0^+_2$ level at N=60 has far too low an energy (we note, that the existence of $\beta$ vibrations in nuclei is being questioned [6, 7, 69–71]).

As mentioned, the $0^+_2$ levels nuclei may result from excitations of nucleon pairs between neighboring orbitals. Figure 10 (a) displays the Nilsson diagram for neutrons in the mass A≈100 region, showing the upslopping $\nu 9/2^+[404]$ extruder, which crosses a number of downslopping orbitals when the Fermi level rises between N=50 and N=60. We propose that a multiple action of the $\nu 9/2^+[404]$ extruder helps creating 2p-2h excita-

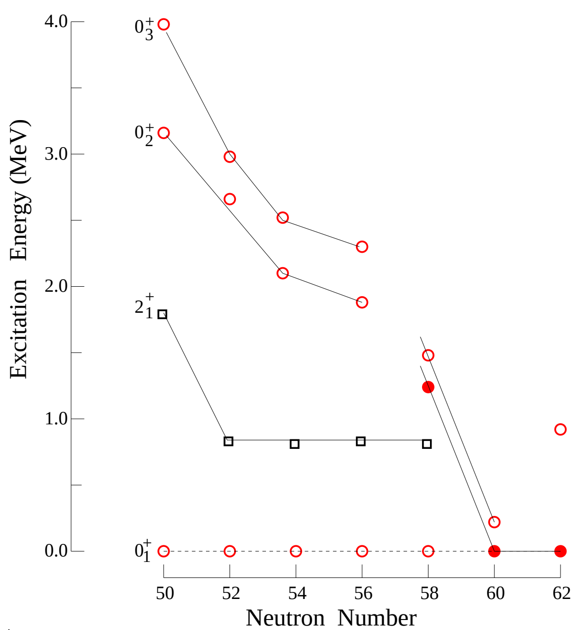


FIG. 9: Excitation energies of $0_2^+$ and $0_3^+$ levels in Sr isotopes. The data are taken from the present work and from the ENSDF base [4]. Lines are drawn to guide the eye. See text for more comments.

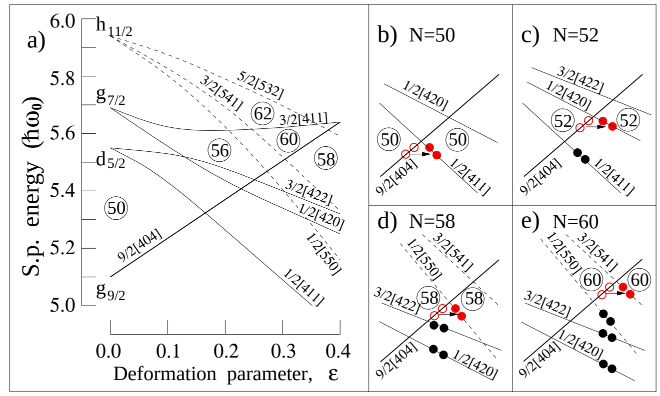


FIG. 10: (a) The Nilsson diagram for neutrons drawn after Fig. 9 of Ref. [55]. Panels (b) - (e) are described in the text.

tions with spin $0^+$ via the "pair-hopping" mechanism [10–12], as drawn schematically in Figs. 10 (b)-(e) showing fragments of Fig. 10 (a), for various N values. Analogous mechanism was employed to explain the low-lying $0^+$ levels in $^{98}$Sr and $^{100}$Zr [1] and in neutron-rich lanthanides where analogous extruders are the $\nu 11/2^-[505]$ and $\pi/2^+[404]$ orbitals [6–8].

At N=50 (Fig. 10 (b)) neutron pair is passed from the occupied $9/2^+[404]$ to the empty $1/2^+[411]$ orbital, creating a $0^+$ level at a rather high energy. With the increasing Fermi level and two neutrons added the $9/2^+[404]$ orbital is filled again. The $0^+$ ground state at N=52 has the $\nu\ g_{9/2}$ shell fully occupied and two neutrons in the $d_{5/2}$ shell. However, at higher excitation another $0^+$ level can be created by transferring a pair of neutrons from the $9/2^+[404]$ extruder to the $\nu\ 1/2^+[420]$ orbital, as shown in Fig. 10 (c). We note, that the $1/2^+[411]$ orbital has properties of the $g_{7/2}$ shell, after crossing with the $1/2^+[420]$ orbital, and can interact with $g_{9/2}$ protons, lowering the excitation of the $0_2^+$ level in $^{90}$Sr.

The multiple action of the $\nu\ g_{9/2}$ extruder, a catalyst of the deformation-driving process, continues as long as it remains active at the Fermi level, crossing subsequent downslopping orbitals. The neutron pair transfer shown in Figs. 10 (b) and (c) is repeated at higher N, building slowly the collectivity. However, at N=58 there is an essential change as a pair of neutrons can be transferred to the *strongly* deformation-driving $1/2^-[550]$ orbital, as shown in Fig. 10 (d). This creates a deformed $0_2^+$ level in $^{96}$Sr. The deformation grows further at N=60, where a pair of neutrons is passed to the $3/2^-[550]$ orbital, as shown in Fig. 10 (e). The interaction with $g_{9/2}$ protons lowers the energy of the $0_2^+$ level such, that it becomes the ground state in $^{98}$Sr.

For the very low-lying, spherical $0_2^+$ level in $^{98}$Sr a more exotic configuration was proposed with a pair of neutrons in the $11/2^-[505]$ orbital present at the Fermi surface on the oblate side of the potential (see Fig. 7 in Ref. [1]). This may explain some puzzling properties of this level - the very low mixing with the $0_1^+$ ground state and numerous decays of the band on top of the $0_2^+$ level to the ground-state band. The $0_3^+$ level in $^{96}$Sr may correspond to the same configuration (see Fig. 5 in Ref. [1]).

Figure 11 compares measured energies of excited $0^+$ levels in Sr isotopes, with the corresponding energies obtained from the LSSM. The calculations reproduce the lowering of $0_{exc}^+$ energies in the 50≤N≤56 range. Curiously, the calculated $0_3^+$ levels follow closely the experimental $0_2^+$ levels whereas the calculated $0_2^+$ levels seem not to have experimental counterparts. However, this may well be a mismatch between experiment and theory. An increase of calculated $0_{exc}^+$ energies by about 0.5 MeV would give a fair agreement between $0_2^+$ levels and a good match between $0_3^+$ levels. To tell more, one should identify experimental $0_4^+$ levels in $^{90,92,94}$Sr nuclei, not known at present.

The situation at N=58 needs special attention. As the $0_2^+$ state in $^{96}$Sr is supposed to be deformed we do not expect it to appear in the present calculations due to a missing deformation- driving mechanism in the model space used. As inferred from previous calculations in Zr [61] and MCSM results [72], at $N = 58$ no deformed structures appear at low energy without addition of the intruders to the present valence space. Also the $0_3^+$ is suggested to be an exotic extruder-hole structure [1]. The calculated $0_2^+$ and $0_3^+$ fairly match the $0_3^+$ and $0_4^+$ experimental levels. The analysis of the wave functions of the computed, $0_2^+$ and $0_3^+$ levels at N=58 shows low population of the SOP orbitals, $\pi g_{9/2}$ and $\nu g_{7/2}$ (see the inset in Fig. 11), which suggests their spherical nature. This is in contrast with the predictions of the Monte-Carlo

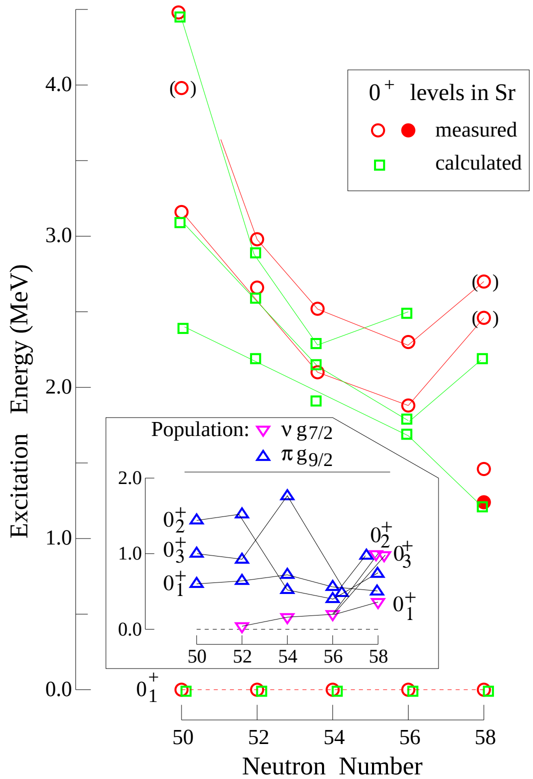


FIG. 11: Comparison of experimental and calculated excitation energies of $0_2^+$, $0_3^+$ and $0_4^+$ levels in Sr isotopes. Filled circle represents a deformed state. The inset is described in the text. The data are taken from this work and Ref. [4]. Lines are drawn to guide the eye.

SM calculations for the deformed states in the zirconium isotopes [72].

The main proton and neutron components in wave functions of levels from the LSSM calculations are named in Table XIV. For example the proton component labelled "**2**" has six $\pi f_{5/2}$ protons, three $\pi p_{3/2}$ protons, one $\pi p_{1/2}$ proton and no $\pi g_{9/2}$ protons. Analogously, the neutron component labelled "**d**" has four $\pi d_{5/2}$ neutrons and no neutrons in other shells.

The dominating components of $0^+$ levels in Fig. 11 expressed in terms of Table XIV are shown in Table XV (we show components for which the probability in the wave function is at least 0.05). For example, the $0_2^+$ level at N=54 has two components, 1d and 4d with probabilities of 0.12 and 0.38, respectively, accounting for 0.50 fraction of the wave function (this summed fraction is shown in the same line as the $0_2^+$ symbol), the remaining 0.50 scattered among components with low amplitudes.

The most important features seen in Table XV are

(i) the complexity of wave functions increasing with growing neutron number. At N=50 the probabilities of the few dominating components sum up to about 0.85, a fraction which drops below 0.5 at N=56.

(ii) the domination of the $\nu d_{5/2}^n$ component, n=N-50, in the wave functions at N<58

TABLE XIV: The list of main proton and neutron components in wave functions of the levels in Sr isotopes as obtained in present LSSM calculations.

| proton component | f5/2 | p3/2 | p1/2 | g9/2 | |
|---|---|---|---|---|---|
| | | positive | parity | | |
| **1** | 6 | 4 | 0 | 0 | |
| **2** | 6 | 3 | 1 | 0 | |
| **3** | 6 | 2 | 2 | 0 | |
| **4** | 6 | 2 | 0 | 2 | |
| **5** | 5 | 4 | 1 | 0 | |
| **6** | 5 | 3 | 0 | 2 | |
| **7** | 5 | 2 | 1 | 2 | |
| **8** | 4 | 4 | 2 | 0 | |
| **9** | 4 | 4 | 0 | 2 | |
| **10** | 4 | 3 | 1 | 2 | |
| **11** | 4 | 2 | 2 | 2 | |
| **12** | 6 | 1 | 1 | 2 | |
| | | negative | parity | | |
| **13** | 6 | 3 | 0 | 1 | |
| **14** | 6 | 1 | 0 | 3 | |
| **15** | 6 | 2 | 1 | 1 | |
| **16** | 6 | 1 | 2 | 1 | |
| **17** | 5 | 4 | 0 | 1 | |
| **18** | 5 | 3 | 1 | 1 | |
| **19** | 5 | 2 | 2 | 1 | |
| **20** | 5 | 2 | 0 | 3 | |
| **21** | 4 | 3 | 2 | 1 | |
| neutron component | d5/2 | s1/2 | g7/2 | d3/2 | h11/2 |
| | | positive | parity | | |
| **a** | 2 | 0 | 0 | 0 | 0 |
| **b** | 1 | 1 | 0 | 0 | 0 |
| **c** | 0 | 2 | 0 | 0 | 0 |
| **d** | 4 | 0 | 0 | 0 | 0 |
| **e** | 3 | 1 | 0 | 0 | 0 |
| **f** | 3 | 0 | 0 | 1 | 0 |
| **g** | 6 | 0 | 0 | 0 | 0 |
| **h** | 5 | 1 | 0 | 0 | 0 |
| **i** | 4 | 2 | 0 | 0 | 0 |
| **j** | 2 | 2 | 0 | 0 | 0 |
| **k** | 5 | 0 | 0 | 1 | 0 |
| | | negative | parity | | |
| **l** | 5 | 0 | 0 | 0 | 1 |
| **m** | 1 | 0 | 0 | 0 | 1 |
| **n** | 3 | 0 | 0 | 0 | 1 |

(iii) the domination of $\pi(f,p)$ components in the wave functions of the $0_1^+$ level

(iv) the increasing population of the $g_{9/2}$ proton orbital with excitation energy and its decrease with the growing neutron number

(v) low population of the $g_{7/2}$ neutron orbital at N<58.

The inset in Fig. 11 shows the summed population of the $\pi g_{9/2}$ and $\nu g_{7/2}$ shells. There is a moderate population of the $g_{9/2}$ proton and very low population of the $g_{7/2}$ neutron shell (at N<58 neutron population is very similar for $0_1^+$, $0_2^+$ and $0_3^+$ levels). Although the occu-

TABLE XV: Structure of $0^+$levels in Sr isotopes in terms of main components listed in Table XIV, as calculated with LSSM in this work. See text for further explanations.

| Level | N=50 | N=52 | N=54 | N=56 |
|---|---|---|---|---|
| $0_1^+$ | 0.84 | 0.65 | 0.46 | 0.40 |
| | **1**, 0.59 | **1a**, 0.33 | **1d**, 0.20 | **1g**, 0.12 |
| | **3**, 0.08 | **2a**, 0.08 | **3d**, 0.11 | **3g**, 0.10 |
| | **4**, 0.11 | **3a**, 0.11 | **4d**, 0.05 | **8g**, 0.18 |
| | **9**, 0.06 | **4a**, 0.07 | **8d**, 0.10 | |
| | | **8a**, 0.06 | | |
| $0_2^+$ | 0.86 | 0.50 | 0.50 | 0.45 |
| | **1**, 0.15 | **1a**, 0.13 | **1d**, 0.12 | **1g**, 0.07 |
| | **3**, 0.05 | **4a**, 0.19 | **4d**, 0.38 | **8g**, 0.38 |
| | **4**, 0.32 | **6a**, 0.06 | | |
| | **6**, 0.08 | **8a**, 0.12 | | |
| | **8**, 0.16 | | | |
| | **9**, 0.05 | | | |
| | **11**, 0.05 | | | |
| $0_3^+$ | 0.83 | 0.62 | 0.32 | 0.49 |
| | **4**, 0.28 | **4a**, 0.16 | **4d**, 0.17 | **1g**, 0.05 |
| | **8**, 0.55 | **8a**, 0.41 | **4f**, 0.06 | **1i**, 0.05 |
| | | **8c**, 0.05 | **8d**, 0.09 | **3g**, 0.05 |
| | | | | **8i**, 0.34 |
| $0_4^+$ | 0.81 | 0.62 | 0.29 | 0.06 |
| | **3**, 0.55 | **1c**, 0.26 | **1j**, 0.14 | **1g**, 0.06 |
| | **7**, 0.09 | **2a**, 0.13 | **8j**, 0.15 | |
| | **8** 0.17 | **3a**, 0.06 | | |
| | | **8a**, 0.06 | | |
| | | **8c**, 0.06 | | |
| | | **9c**, 0.05 | | |

pancy of $\nu g_{7/2}$ and $\pi g_{9/2}$ orbitals increase at $N = 58$, it is still much below of what is expected in the highly deformed states (see Ref. [72]).

The above results indicate that the structure of excited $0^+$ levels at N<58 is dominated by the $\pi(f,p)\otimes\nu d^n_{5/2}$ configuration admixed by $g_{9/2}$ protons at higher energy but not by $g_{7/2}$ neutrons. Thus, the SOP mechanism does not work at N<58, while the $\nu d^n_{5/2}$ component supports the extruder action shown in Figs. 10 (b) and (c).

Finally, let us comment on other studies of $0^+$ levels in Sr isotopes. The deformed band on top of the $0_2^+$ level in $^{96}$Sr, proposed in Ref. [33], was also reported by Coulomb-excitation studies [43, 44] where, in addition, a deformed band on top of the $0_3^+$ level at 1464.6 keV was suggested (not observed to date). In Ref. [45] larger fraction of the spherical configuration was attributed to the $0_2^+$ level than to the $0_3^+$ level in $^{96}$Sr, whereas the present work suggest the opposite. It was also suggested that the $0_2^+$ state in $^{98}$Sr is similar to the $0_1^+$ ground state in $^{96}$Sr [46], albeit contradicting their shell-model calculations. As discussed above, we propose that the

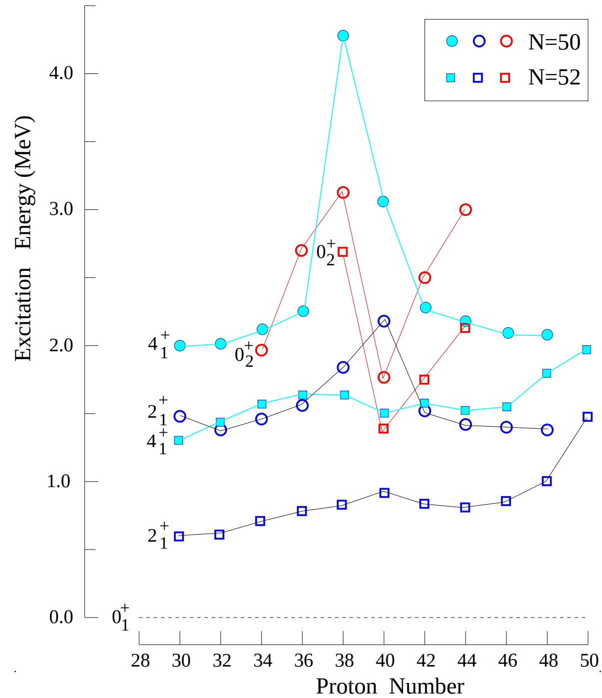


FIG. 12: Excitation energies of low-spin levels in N=50 and N=52 isotones. The data are from the present work and from the ENSDF base [4]. Lines are drawn to guide the eye.

$0_2^+$ level in $^{98}$Sr is similar to the $0_3^+$ level in $^{96}$Sr. We agree with Ref. [46] that the Monte Carlo shell-model calculations [72] predict the onset of deformation in Sr isotopes at too low a neutron number. In Ru isotopes where the collectivity is higher than in Sr isotopes (see Fig. 1) a weakly deformed band on top of the $0_2^+$ level was recently reported in $^{98}Ru_{54}$ [73].

### C. $2^+$ excitations

A low-energy, $2_1^+$ state, the most common type of excitation in nuclei is still an enigmatic phenomenon. As remarked in Ref. [71], "the phonon interpretation of the low-energy nuclear structure remains controversial". In Ref. [12] the $2_1^+$ excitations were called a "genuine quantum vibrations that are essentially different from surface oscillations of a classical liquid drop".

Figure 12 displays low-energy, positive-parity excitations as a function of the proton number, Z. This picture and Fig. 8 show significant variations of $2_1^+$ excitation energies along both, Z and N. The $2_1^+$ energy is nearly two times higher at N=50 (no valence neutrons) than at N=52. Furthermore, in N=50 isotones the $2_1^+$ energy clearly increases at the Z=40 proton subshell closure, which is not seen at N=52, where the pair of neutrons dilutes the effect (there is still a strong variation of the $0_2^+$ energy at N=52). Large variations of the $2_1^+$ energy seen in Figs. 8 and 12 suggest that this is not any phonon-type excitation because a phonon, expected to be a complex excitation, should not show such rapid variations. Also the $R_{4/2}$ ratio of $2_1^+$ and $4_1^+$ excitation energies in the discussed nuclei does not support a two-phonon nature of the $4_1^+$ levels shown. The figures indicate that both, protons and neutrons contribute to these excitations and suggest that they are, predominantly, a few valence nucleons additionally "dressed in collectivity" [12] by coupling to a giant monopole, quadrupole and pairing vibrations [74–76]. Such coupling is supported by the observation that collectivity is fragmented among higher-lying $2^+$ levels as seen in the neighboring Kr isotopes at N=50 and N=52 [77]. Low collectivity of $2_1^+$ levels in $^{90-96}$Sr isotopes is further indicated by small B(E2;$2_1^+ \rightarrow 0_1^+$) rates [78].

### 1. *Structure of $2^+$ levels*

In Ref. [1] we proposed a phenomenological classification of $0^+$ excitations, where 57 out of 63 known $0_2^+$ and $0_3^+$ levels from the 38≤Z≤50, 52≤N≤66 region follow regular "parabolic" trends along the proton number. Analogous "parabolas" were obtained theoretically in the IBM-CM calculations of the "intruder" $0^+$ levels in the region [68] (see Fig. 4 there).

Apparently, $2^+$ excitations in Sr isotopes and their neighbors also can be arranged along "parabolas" in function of N, facilitating the understanding of various features shown in Fig. 8. Figure 13 shows three groups of such "parabolas". We propose that each group corresponds to a specific proton configuration while the "U" shape within a group results from the Fermi level crossing a neutron shell. The regular trends seen in Fig. 13 involve 47 out of 53 known $2_1^+$, $2_2^+$ and $2_3^+$ levels in the (32≤Z≤38, 50≤N≤60) region. The six remaining cases are discussed below.

We propose that the $2^+$ levels represented by open circles correspond to excitations within the $d_{5/2}$ neutron shell. In the 50≤N≤54 range these points correspond to $2_1^+$ levels but when the Fermi level approaches N=56, energies of these levels increase and they become $2_2^+$ excitations. It is expected that the proton configuration in this group has the lowest energy. Filled squares may correspond to the same neutron configuration coupled to a higher-energy proton excitation. The points represented by open squares, being $2_1^+$ levels at N=56 and N=58, $2_2^+$ excitations at N=54 and $2_3^+$ excitations at N=52, may correspond to filling other neutron shells.

To learn more we performed LSSM calculations for $2^+$ excitations in Sr isotopes. Figure 14 compares measured and calculated energies of $2_1^+$, $2_2^+$ and $2_3^+$ levels in $^{88,90,92,94,96}$Sr nuclei. The calculated points follow closely the experimental "parabolic" trends. In the figure four distinct groups of data points. One may ask whether the LSSM calculations predict similar configurations within each groups.

Dominating structures of the configurations in Fig. 14, calculated at N= 50, 52, 54 and 56 are shown in Table

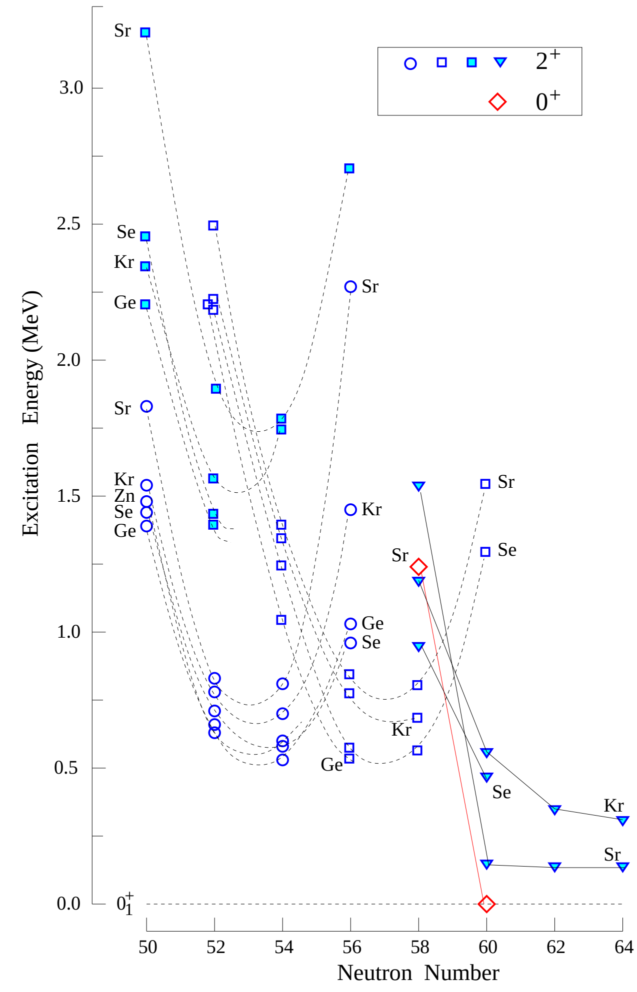


FIG. 13: Excitation energies of $2_1^+$, $2_2^+$ and $2_3^+$ levels in Zn, Ge, Se, Kr and Sr isotopes. The data are taken from the present work and from the ENSDF base [4]. Lines are drawn to guide the eye. See text for further comments.

XVI. For each configuration we show the most important components, for which the probability in the wave function is at least 0.05. For example, the $2_1^+$ level at N=54, has three components, 1d, 2d and 3d with probabilities of 0.17, 0.07 and 0.10, respectively, which sum up to 0.34. We note that this configuration has a simple structure of dominating components, which can be written as $(1{+}2{+}3)\otimes\nu d^n_{5/2}$, where n=N-50. We assign label A to this configuration. It describes $2_1^+$ levels at N=52 and N=54. Analogously, configuration B assigned to the $2_1^+$ level at N=56 in TableXVI can be written as $(2{+}5{+}8)\otimes\nu d^n_{5/2}$.

At higher excitation energies the configurations mix and acquire more components with lower amplitudes. Notably, the $2_2^+$ levels at N=54 and N=56 are mixtures of configurations A and B. A remarkable result of this work is the demonstration that the crossing in the experimental systematics of excitation energies between configura-

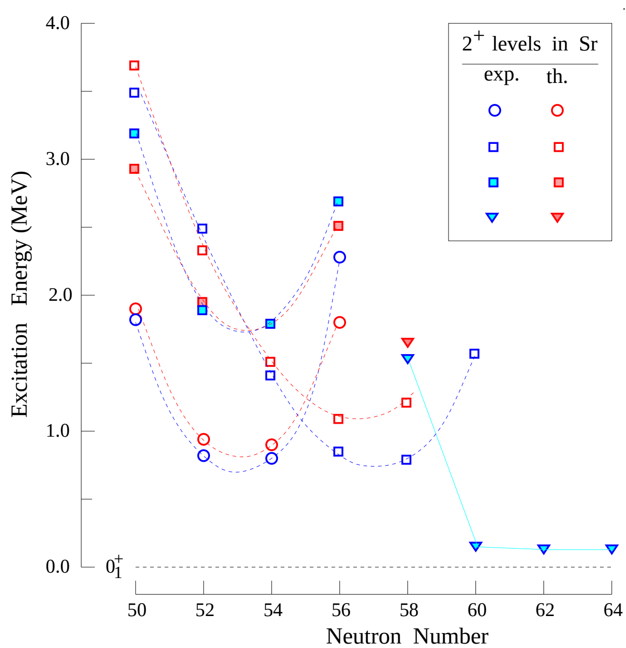


FIG. 14: Comparison of excitation energies of $2_1^+$, $2_2^+$ and $2_3^+$ levels in Sr isotopes observed experimentally (blue symbols) and calculated within LSSM (red symbols). The data are taken from the present work and from the ENSDF base [4]. Lines are drawn to guide the eye.

TABLE XVI: The structure of $2_1^+$, $2_2^+$ and $2_3^+$ levels in Sr isotopes in terms of components listed in Table XIV, as calculated with LSSM in this work. See text for further comments.

| Level | N=50 | N=52 | N=54 | N=56 |
|---|---|---|---|---|
| $2_1^+$ | 0.76 | **A**, 0.53 | **A**, 0.34 | **B**, 0.23 |
| | **2**, 0.34 | **1a**, 0.28 | **1d**, 0.17 | **2g**, 0.08 |
| | **5**, 0.35 | **2a**, 0.14 | **2d**, 0.07 | **5g**, 0.09 |
| | **8**, 0.07 | **3a**, 0.11 | **3d**, 0.10 | **8g**, 0.06 |
| $2_2^+$ | 0.89 | 0.49 | **B+A**, 0.42 | **B+A**, 0.41 |
| | **2**, 0.38 | **1a**, 0.05 | **2d**, 0.16 | **1h**, 0.05 |
| | **5**, 0.39 | **1b**, 0.09 | **3d**, 0.05 | **5g**, 0.10 |
| | **7**, 0.06 | **2a**, 0.15 | **5d**, 0.16 | **8g**, 0.10 |
| | **10**, 0.06 | **5a**, 0.20 | **bd**, 0.05 | **8h**, 0.16 |
| $2_3^+$ | 0.71 | **A+B**, 0.44 | 0.40 | 0.31 |
| | **4**, 0.60 | **1a**, 0.05 | **1e**, 0.17 | **2g**, 0.13 |
| | **6**, 0.05 | **1b**, 0.17 | **8e**, 0.11 | **5g**, 0.05 |
| | **9**, 0.06 | **2**a, 0.05 | **2d**, 0.06 | **8h**, 0.13 |
| | | **5a**, 0.17 | **3e**, 0.06 | |

tion A and B (blue circles and squares on blue "parabolas" in Fig. 14) is reproduced by the calculated structures of the corresponding $2^+$ levels. The $2_1^+$ level, which has the configuration A at N=52 and N=54 (red circles) changes its structure to configuration B (red square) at N=56, while the $2_2^+$ level, which has the dominating configuration B at N=54 (red square) acquires an admixture of configuration A at N=56 (red circle). This explains the "unusual" position of the $2_2^+$ level of $^{96}$Sr in Fig. 8.

It is of interest to extend such Shell Model analysis to $2^+$ levels in other isotopic lines displayed in Fig. 13, which showing experimental systematics similar to those of Sr isotopes.

### *2. $2_1^+$ levels and the deformation*

Figure 13 reveals another interesting effect. The points shown by filled triangles correspond to $2^+$ excitations in rotational bands and display trend (seen most clearly in Sr isotopes) where the $2_2^+$ level rapidly drops in energy (from 1507.0 keV in $^{96}$Sr to 144.6 keV in $^{98}$Sr) and continues as the $2_1^+$ rotational level (positions of corresponding $0^+$ band heads are marked by red diamonds). The $2_1^+$ levels at N≥60 and $2_2^+$ levels in $^{92}$Se and $^{94}$Kr at N=58, shown by filled triangles, belong to the same category. One notes, that the $2_1^+$ energy in $^{94}$Se is lower than in $^{96}$Kr. Thus, the collectivity in Se isotopes may be higher than in Kr isotopes, contrary to claims of Ref. [79] that Kr isotopes mark the low-Z boundary of the deformation at N=60 (it is of a high interest to find the $2_1^+$ excitation energy in $^{96}Se_{62}$). This is supported by Ref. [62] (see Fig. 1 there) suggesting an increase of collectivity below Z=36. As noted there the tensor mechanism proposed in Ref. [72] does not work at Z<38, so the collectivity should have another origin.

The evolution in Kr isotopes seen in Fig. 13 is characteristic of the second-order phase transition [80, 81], where the $2_1^+$ energy drops gradually and there is no crossing with a deformed $0_2^+$ configuration. More generally, the deformation change around the neutron number N=60 corresponds primarily to the second-order phase transition (gradual increase of collectivity in the ground-state configuration with the increasing neutron number) and is observed in a wide range of protons, from Se (possibly Ge) to Pd, with maximum collectivity in Mo isotopes. However, on top of this change superimposed is another contribution to the shape change, which is due to the first-order phase transition [80, 81], helped here by the $\nu 9/2^+[404]$ extruder, generating coexisting, deformed $0^+$ configurations in Sr and Zr [1]. The two contributions added are responsible for a sudden deformation onset observed at N=60 in $^{98}$Sr and $^{100}$Zr nuclei. This picture is supported by the evolution of the mean-square charge radii and the two-neutron separation energies in the region [68, 82, 83], which are sensitive probes of collectivity [84–86]. As seen in Fig. 1 of Ref. [82], Fig. 2 of Ref. [68] and Figs. 3 and 4(a) of Ref. [83] there is an extra variation of these two observable in Rb, Sr, Y, Zr and Nb isotopes around neutron number N=59, which is where the $9/2^+[404]$ neutron extruder is observed at the Fermi level [48, 55, 59, 60, 87–91].

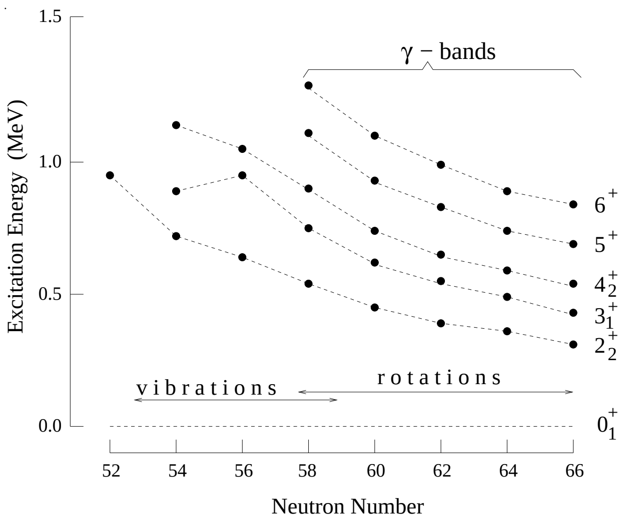


FIG. 15: Evolution of $\gamma$ bands in Ru isotopes. Data are taken from Ref. [3] and the ENSDF base [4].

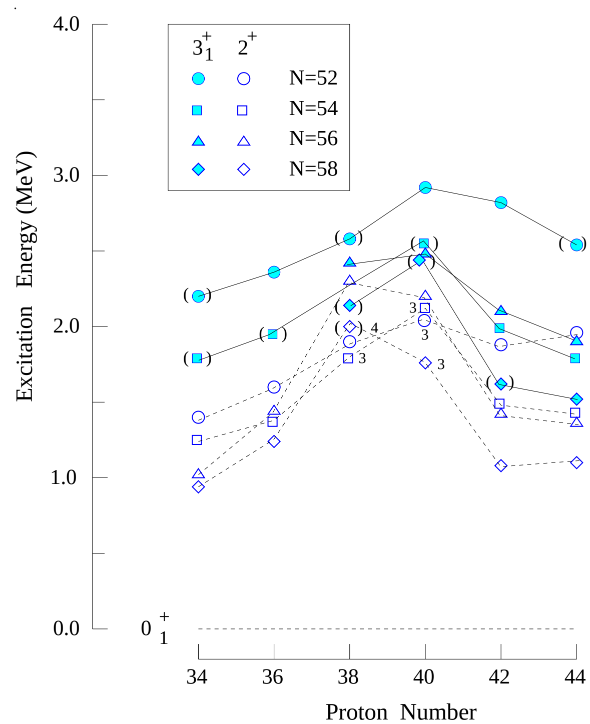


FIG. 16: Excitation energies of $3^+_1$ (filled symbols) and related $2^+$ (empty symbols) levels in N=52, 54, 56 and 58 isotones. In five cases the $2^+_3$ and $2^+_4$ levels are shown. Data with non-unique spin-parity assignments are shown in parentheses. The data are taken from this work and Refs. [4, 63, 64, 99].

### D. $\gamma$ vibrations vs. mixed-symmetry states

The, so called, $\gamma$ excitations, which are $2^+$ levels with K=2 projection on the symmetry axis, are commonly reported at low energies. In many nuclei they are identified with $2^+_2$ levels and are believed to be collective modes with bands on top of them. The most spectacular $\gamma$ bands in the region are reported in Mo [92] and Ru nuclei [93] with the best-to-date candidate for a harmonic, two-phonon $\gamma$-vibrational state in $^{106}$Mo [94]. In spherical nuclei, with no symmetry axis defined, the K=2 excitations are not expected. Still one observes there $2^+$ levels, which evolve smoothly into $\gamma$ bands at higher N, as illustrated in Fig. 15 for Ru isotopes.

Apart from the K=2 projection, another specific feature of a $\gamma$ band is the $3^+$ excitation within the band. Its position relative to the $2^+$ and $4^+$ in-band levels allows distinguishing between vibrational or rotational character of the band [95–97], though with some doubts [98].

Numerous $3^+$ levels in the region were reported [63, 64, 99] with the recent example of both, vibrational and rotational $\gamma$ bands in $^{100}$Zr and $^{102}$Z [100]. The data from Fig. 8 of Ref. [64], including $3^+$ levels from excitation schemes in Figs. 3, 5 and 7, are shown in Fig. 16, for the N=52, 54, 56 and 58 isotones. In the figure we also show $2^+$ excitations, which are related to $3^+$ levels. In most cases these are $2^+_2$ levels but for $^{92}$Sr, $^{92}$Zr, $^{94}$Zr and $^{98}$Zr, where the $2^+_2$ level is not connected with the $3^+$ level, we have show $2^+_3$ levels and in $^{96}$Sr the $2^+_4$ level.

All four isotonic lines show similar pattern with $2^+$ and $3^+$ energies increasing with the growing proton number up to Z=38 or Z=40 and then decreasing. Both $2^+$ and $3^+_1$ energies decrease with the growing neutron number. These similarities and regularities suggest that the levels shown in Fig. 16 belong to the same excitation mode, which in Mo and Ru nuclei is identified as $\gamma$ excitation.

In Fig. 17 the calculated energies of $3^+_1$ levels in Sr isotopes are compared to their experimental counterparts. We show, in addition, experimental levels for Mo and Ru isotopes, where $3^+_1$ levels are identified as members of $\gamma$ bands. The similarity between systematic trends shown by the Sr, Mo and Ru data along N suggests that the $3^+_1$ levels in Sr isotopes have a similar structure as those in Mo and Ru isotopes. This is in contrast to the shell-model calculations of Ref. [41] where it was concluded that the $3^+_1$ level at 2421.50 keV in $^{94}$Sr$_{56}$ is predominantly a single-particle excitation.

The calculated excitation energies (red circles) follow closely the experimental data. In $^{92}$Sr, where the experimental $3^+_1$ level is not known, the calculations predict an excitation energy of 2.05MeV, in accord with the downsloping trend in Mo and Ru.

We have also checked the quadrupole properties of the calculated $3^+_1$ levels in the Sr chain. In $^{92}$Sr the spectroscopic quadrupole moment, $Q(3^+_1) = 2.2 e^2 fm^2$, approaches the zero value expected for a $K = 2$ band. Furthermore, the $3^+_1$ and the second excited $2^+_2$ state are connected by a strong $E2$ transition of $B(E2; 3^+ \rightarrow 2^+_2) = 319 \mathrm{e^2fm^4}$ (for comparison, $B(E2; 2^+ \rightarrow 0^+_{gs}) = 224 \mathrm{e^2fm^4}$). This and the lowering of the computed $3^+_1$ energy as a function of N suggests some non-axiality at $N = 54$. It is worth noting that the same LSSM calculations predicted triaxial deformation at in Se and Ge

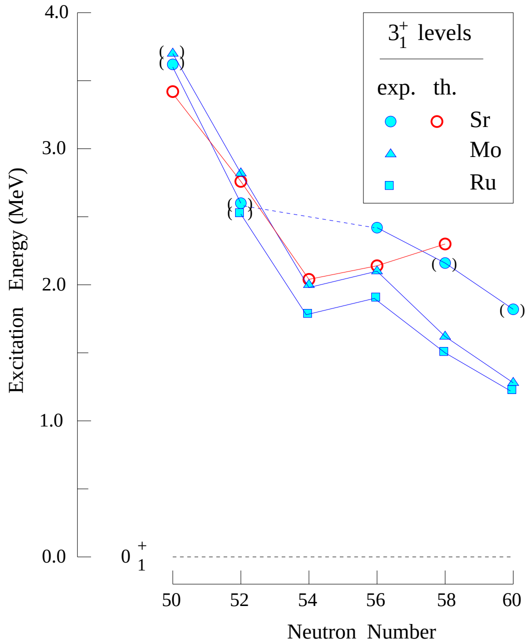


FIG. 17: Experimental excitation energies of $3_1^+$ levels in the 50≤N≤58 isotopes of Sr (filled blue circles) compared to the LSSM calculated energies (empty red circles). Experimental energies for $3_1^+$ levels in isotopes of Mo (filled blue triangles) and Ru (filled blue squares) are shown for comparison. Data points with non-unique or tentative spin-parity assignments are shown in parentheses. The experimental data are taken from the present work and the ENSDF base [4].

isotopes with $N = 52, 54$ [101].

In Table XVII structures of calculated $3_1^+$ levels in Sr isotopes are expressed in terms of dominating components. Comparing structures of $3^+$ levels from Table XVII with structures of $2^+$ levels from Table XVI one sees that the dominating components in wave functions of $3_1^+$ levels are closer to those of $2_2^+$ levels than of other $2^+$ levels. The systematic trend in Fig. 17 even resembles the crossing between two "parabolas" for $2_2^+$ and $2_3^+$ levels in Fig. 14 with the $3_1^+$ configurations at N=52 and N=54 having more low amplitude components than at N=50 and N=56, which may reflect configuration mixing at the crossing. Indeed, the $3_2^+$ level at 2.92 MeV (0.15 MeV above $3_1^+$) in $^{90}Sr_{52}$ has a very similar structure to the structure of $3_1^+$ levels in $^{90}$Sr and $^{92}$Sr.

Interestingly, at N=56 the $3_2^+$ state predicted at 2.86 MeV, is dominated by a neutron excitation to the $d_{3/2}$ orbital whose *total* occupation reaches 0.77 particle. The same population of the $d_{3/2}$ orbital is predicted in the $3_1^+$ level at N=58, where in addition the total occupation of the $g_{7/2}$ orbital grows to 0.6. However, the the sum of the dominating components is 0.32, only, indicating a continuous increase of collectivity with N. At the same time, the proton structure of the $3^+$ levels remains nearly unchanged along the chain, with the $g_{9/2}$ occupation around 0.5 particle. As for $2^+$ levels, the total population of the

TABLE XVII: Structure of $3^+$ levels in Sr isotopes in terms of main components listed in Table XIV, as calculated with LSSM in this work. See text for further comments.

| Level | N=50 | N=52 | N=54 | N=56 |
|---|---|---|---|---|
| $3_1^+$ | 0.93 | 0.61 | 0.54 | 0.50 |
| | **5**, 0.81 | **1b**, 0.15 | **1d**, 0.20 | **1h**, 0.11 |
| | **7**, 0.06 | **2a**, 0.17 | **2d**, 0.09 | **3h**, 0.09 |
| | **10**, 0.06 | **2b**, 0.07 | **3d**, 0.12 | **8h**, 0.30 |
| | | **5a**, 0.11 | **8d**, 0.13 | |
| | | **5b**, 0.06 | | |
| | | **8b**, 0.05 | | |
| $3_2^+$ | | 0.53 | 0.37 | 0.26 |
| | | **1b**, 0.23 | **5d**, 0.11 | **1k**, 0.12 |
| | | **2a**, 0.09 | **8d**, 0.06 | **3k**, 0.06 |
| | | **5a**, 0.14 | **1e**, 0.11 | **8k**, 0.08 |
| | | **8b**, 0.07 | **8e**, 0.09 | |

$\nu g_{7/2}$ shell in $3^+$ levels at N<58 is negligible.

The observed proximity of two $3^+$ configurations is expected in this region, where apart of $\gamma$ excitations mixed symmetry states, $2_m^+$, which are proton-neutron isovector excitations [102–104], are reported at N=52 and N=54 in $^{92}$Zr [105], $^{94}$Mo [106–109], $^{96,98}$Mo [110] and $^{96}$Ru [111]. The quadrupole collective mode, $Q_m$, generating mixed-symmetry states, coupled to the $2_1^+$ state (the symmetric, $Q_s$, mode) produces a quintuplet of two-phonon states, $Q_mQ_s|0_1^+>$, with spins from $0^+$ to $4^+$, which decay by enhanced M1 transitions to $0^+$, $2^+$ and $4^+$ states of the two-phonon, symmetric triplet ($Q_sQ_s$).

The characteristic signature of the $Q_mQ_s|0_1^+>$ quintuplet is the low-energy $1^+$ excitation. Figure 18 shows known experimental levels with spin $1^+$ in Sr isotopes with 50≤N≤58. For comparison we show $1^+$ levels in Zr, Mo and Ru isotopes. There is a general decrease of $1^+$ excitation energies with the growing neutron number. The LSSM calculations shown in Fig. 18, reproduce well the $1^+$ energy in $^{88}Sr_{50}$ and are close to $1^+$ energies in Zr, Mo and Ru nuclei at N=52 (experimental $1^+$ level in $^{90}Sr_{52}$ is not know). The trend in Fig. 18 resembles the trend of $3_1^+$ levels in Fig. 17, suggesting some relation between $1_1^+$ and $3_1^+$ states.

However, $1^+$ states may have another origin. The $1^+$ excitation with enhanced M1 decay seen in $^{86}K_{50}$ [57] does not involve valence neutrons. As discussed in the review work [112], $1^+$ excitations may appear due to coupling with high-energy modes. Furthermore, as argued in Ref. [61] the LSSM calculations produce more complex wave functions in these nuclei than expected for a pure $Q_s|0_1^+>$, $Q_m|0_1^+>$ state. One may also note, that at N=50 the $1_1^+$ energy in $^{88}$Sr is significantly lower than in $^{90}$Zr (4.6 MeV) and is close to that in $^{86}$Kr (2926 keV). This suggests that below Z=40 the $1_1^+$ levels at N=50 are

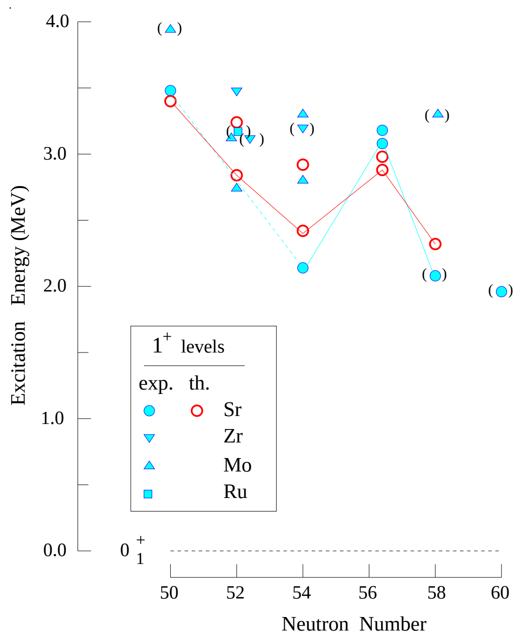


FIG. 18: Experimental excitation energies of $1^+$ levels in the 50≤N≤58 Sr isotopes compared to the LSSM calculated energies. Experimental $1^+$ levels in isotopes of Zr, Mo and Ru are shown for comparison. The data with tentative spin-parity assignments are shown in parentheses. The experimental data are taken from the present work and Ref.[4].

TABLE XVIII: Structure of $1^+$ levels in Sr isotopes in terms of components from Table XIV, as obtained in this work.

| Level | N=50 | N=52 | N=54 | N=56 |
|---|---|---|---|---|
| $1^+_1$ | 0.97 | 0.64 | 0.47 | 0.46 |
| | **2**, 0.78 | **2a**, 0.25 | **1e**, 0.19 | **2h**, 0.06 |
| | **7**, 0.07 | **5a**, 0.32 | **2e**, 0.08 | **5h**, 0.25 |
| | **10**, 0.06 | **8a**, 0.07 | **3e**, 0.07 | **8h**, 0.15 |
| | **12**, 0.06 | | **8e**, 0.13 | |
| $1^+_2$ | 0.84 | 0.57 | 0.44 | 0.36 |
| | **4**, 0.69 | **2a**, 0.50 | **2d**, 0.27 | **2g**, 0.30 |
| | **6**, 0.08 | **5a**, 0.07 | **8d**, 0.06 | **1k**, 0.06 |
| | **12**, 0.07 | | **1f**, 0.06 | |

due to s.-p. proton excitations within $\pi(f,p)$ shells.

Figure 19, which is analogous to Fig. 17 of Ref. [57], shows in panel (a) low-spin levels in $^{88}$Sr drawn after the compilation [113] and in panel (b) a schematic decay pattern between mixed-symmetry ($Q_m, Q_mQ_s$) and symmetric ($Q_s, Q_sQ_s$) excitations, dominated by strong M1 transitions [102]. As in case of $^{86}$Kr, basic components of the pattern shown in Fig. 19(b) are present in Fig. 19(a) (though with rather high energies of $Q_sQ_s$ states).

Table XVIII shows the LSSM configurations for $1^+$ levels in Sr isotopes. At N=50 a few single-particle excitations constitute about 90% of wave functions, but the

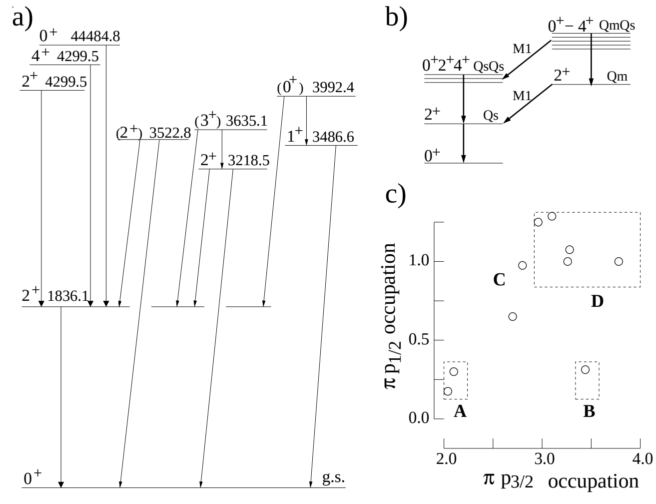


FIG. 19: (a) partial scheme of low-spin excitation in $^{88}$Sr drawn after the compilation [113], (b) a schematic pattern of decays between mixed-symmetry and symmetric excitations, (c) occupation of $\pi p_{3/2}$ and $\pi p_{1/2}$ orbitals calculated for levels of $^{88}$Sr. The A, B, C and D labels are explained in the text.

TABLE XIX: $B(M1)$ values (in $\mu_N^2$ units) for selected transitions in $^{88}$Sr and $^{90}$Sr obtained in the LSSM calculations.

| $J^\pi_f \rightarrow J^\pi_i$ | $B(M1;^{88}Sr)$ | $B(M1;^{90}Sr)$ |
|---|---|---|
| $2^+_2 \rightarrow 2^+_1$ | 0.06 | 0.17 |
| $2^+_3 \rightarrow 2^+_2$ | 0.013 | 0.07 |
| $3^+_1 \rightarrow 4^+_1$ | 0.35 | 0.0004 |
| $1^+_1 \rightarrow 2^+_2$ | 0.05 | 0.05 |
| $1^+_1 \rightarrow 2^+_3$ | 0.04 | 0.075 |

dominating $\pi(f,p)$ configurations are different than in $3^+$ levels. In contrast, at N=52 single-particle excitations have a similar $\pi(f,p)$ configuration in $1^+_1$ and $3^+_1$ levels. This suggests the proton-neutron, mixed-symmetry excitations in $^{90}$Sr$_{52}$. The properties of $^{88}$Sr suggest that the "skeleton" of this pattern is formed at N=50 by single-particle excitations and then additionally "dressed" by the mixed-symmetry collectivity at N=52.

Table XIX shows $B(M1)$ transition rates obtained from LSSM for transitions between low-spin excitations in $^{88}$Sr and $^{90}$Sr. The $2^+_2$ level in $^{90}$Sr could be identified as a mixed-symmetric due to its high B(M1;$2^+_2 \rightarrow 2^+_1$) value and a relatively low B(E2;$2^+_2 \rightarrow 0^+_1$) = 48e$^2$fm$^4$. Nonetheless, the remaining B(M1)s are not supporting the mixed-symmetry character of any other of the excited states. The LSSM calculation suggests the dominating single-particle character of the $1^+$ and $3^+$ levels in $^{88}$Sr, with some admixture of quadrupole collectivity at N=52.

As shown in Fig. 19(c) the occupation of $\pi p_{1/2}$ and $\pi p_{3/2}$ orbitals is correlated in the $\pi p_{1/2}$ vs. $\pi p_{3/2}$ plane,

TABLE XX: Occupation of proton orbitals in selected levels of $^{88}$Sr. See the text for more comments.

| $I^\pi$ | $E_{exc}(keV)$ | $f_{5/2}$ | $p_{3/2}$ | $p_{1/2}$ | $g_{9/2}$ | Group |
|---|---|---|---|---|---|---|
| $0^+_1$ | 0 | 5.64 | 3.44 | 0.31 | 0.62 | **B** |
| $2^+_1$ | 1892 | 5.21 | 3.28 | 1.08 | 0.43 | **D** |
| $0^+_2$ | 2374 | 5.21 | 2.70 | 0.64 | 1.44 | **C** |
| $2^+_2$ | 2945 | 5.32 | 3.26 | 1.01 | 0.42 | **D** |
| $0^+_3$ | 3013 | 4.59 | 3.11 | 1.29 | 1.01 | **D** |
| $1^+_1$ | 3209 | 5.77 | 2.80 | 0.98 | 0.45 | **C** |
| $3^+_1$ | 3416 | 4.86 | 3.78 | 1.00 | 0.36 | **D** |
| $2^+_3$ | 3713 | 5.56 | 2.08 | 0.29 | 2.07 | **A** |
| $4^+_1$ | 3961 | 4.73 | 2.97 | 1.26 | 1.04 | **D** |
| $2^+_4$ | 4065 | 5.49 | 2.22 | 0.43 | 1.86 | **A** |
| $4^+_2$ | 4367 | 5.45 | 1.98 | 0.17 | 2.10 | **A** |

similarly as observed in $^{86}$Kr. By analogy to Fig. 17(b) of Ref. [57], we distinguish in Fig. 19(c) four groups of data points, labelled A, B, C and D (group C is less distinct here than in $^{86}$Kr). Table XX shows occupation probabilities of proton orbitals in low-spin levels of $^{88}$Sr. Labels A, B, C and D are assigned to the respective levels in Table XX) to facilitate the comparison with analogous occupations in $^{86}$Kr, shown in Table X of Ref. [57]. The correlated populations of $\pi p_{1/2}$ and $\pi p_{3/2}$ proton shells produce at N=50 an excitation pattern shown in Fig. 19(a), which is the "skeleton" for mixed-symmetry excitations. At N>50 it acquires some extra collectivity due to p-n coupling.

### E. Negative-parity excitations in Sr isotopes

Figure 20 shows excitation energies of $3^-$ and $5^-$ levels in Kr, Sr, Zr and Mo isotopes of the region, revealing some systematic trends. Excitation energies of $3^-_1$ levels decrease with the increasing neutron number in all the nuclei shown. This suggests an increase of octupole correlations with the increasing neutron number. However, as seen in Figs. 5 and 7, the population of negative-parity levels in $^{96}$Sr is lower than in $^{94}$Sr and the $3^-$ level is not known in $^{98}$Sr, which may be, partly, due to its non-yrast character increasing with N.

In addition to the isoscalar octupole phonon observed in the region [114] the isovector, $3^-$ excitation [115] as well as s.-p. configurations of negative parity appear at similar energies. For example $5^-_1$ levels in $^{90}$Zr and $^{92}$Mo were interpreted as the proton $(g_{9/2}p_{1/2})_{5^-}$ s.-p. coupling and Fig. 20 shows more such levels (points connected by dashed lines). Their excitation energies increase with the increasing neutron number, in contrast to other $5^-$ levels, which probably correspond to the $2^+\otimes 3^-$ coupling. The $5^-_1$ levels in Sr isotopes show an irregular trend and it is not obvious to which configuration they belong - there are close-lying $5^-_2$ levels in $^{92}$Sr and $^{94}$Sr and it is possible that the two configurations mix.

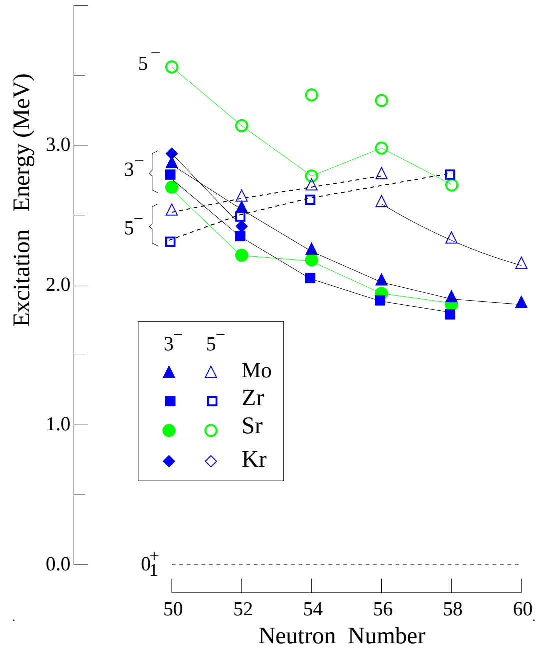


FIG. 20: Experimental excitation energies of negative-parity levels in Sr isotopes compared to LSSM calculations. The data are taken from this work and the ENSDF base [4].

Figure 21 compares experimental excitation energies of low-spin, negative-parity levels in Sr isotopes in the 50≤N≤58 range (filled, green symbols) with energies obtained in the LSSM calculations (empty, red symbols). The LSSM results reproduce the observed excitation energies on average, with the exception of $3^-$ states for which the theory predicts strong increase of their excitation energy with $N$. This suggests an octupole collectivity setting in towards heavier isotopes, which can not be accounted for by the present calculations. Indeed all calculated energies increase at the N=56 subshell closure, which suggests that the calculated levels are of a more single-particle character than experimental levels.

The dominating components of the corresponding wave functions obtained from LSSM are shown in Table XXI. The calculated configurations are dominated by a few components, though their summed contribution drops with N. One notes the increase of negative- parity neutron components at higher N. Another effect is the increasing contribution of dominating components with growing spin, seen at N=56. The inset in Fig. 21 shows the total population of the $\pi g_{9/2}$ and $\nu h_{11/2}$ unnatural-parity shells. This population supports the single-particle character of the $9^-_1$ level in the region [18], with the $\nu h_{11/2}$ contribution increasing with N.

In the discussed region one observes negative-parity excitations above the $9^-_1$ level. They correspond to fully-aligned, two- or four-quasiparticle configurations, providing information on high-$j$ orbitals. The example is the $17^-$ level in $^{98}$Zr corresponding to the $[\pi(g_{9/2})^2\otimes\nu(g_{7/2}h_{11/2})]_{17^-}$ configuration [61, 116]. In the present

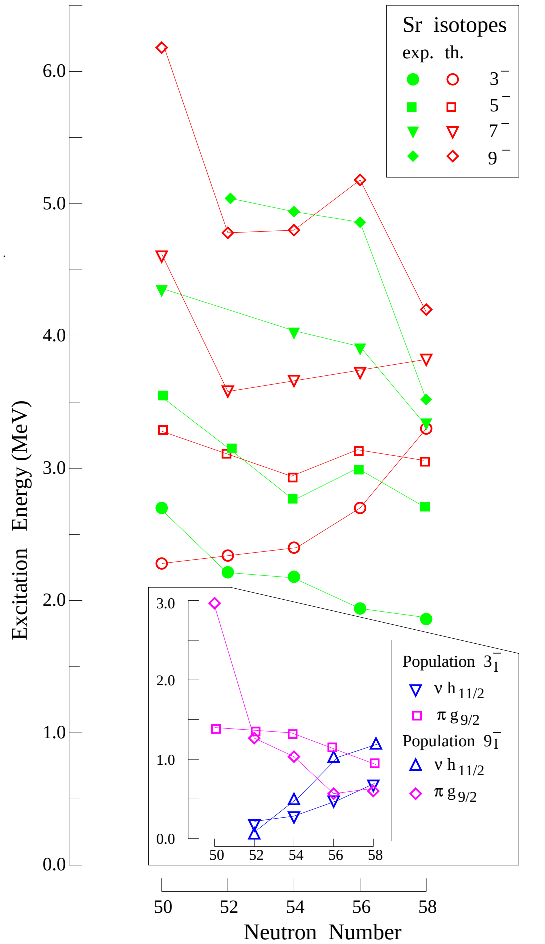


FIG. 21: Experimental energies of negative-parity states (filled green symbols) vs. LSSM calculated energies (empty red symbols) in Sr isotopes. The inset is described in the text. The data are from this work and the ENSDF base [4].

TABLE XXI: Structure of negative-parity levels in Sr isotopes in terms of dominating components listed in Table XIV, as calculated with LSSM in this work.

| $I^\pi$ | N=50 | N=52 | N=54 | N=56 |
|---|---|---|---|---|
| $3_1^-$ | 0.84 | 0.51 | 0.39 | 0.37 |
| | **13**, 0.71 | **13a**, 0.38 | **13d**, 0.23 | **13g**, 0.13 |
| | **14**, 0.08 | **15a**, 0.08 | **15d**, 0.06 | **16g**, 0.05 |
| | **20**, 0.05 | **1m**, 0.05 | **16d**, 0.05 | **21g**, 0.07 |
| | | | **1n** , 0.05 | **1l**, 0.07 |
| | | | | **8l**, 0.05 |
| $4_1^-$ | 0.81 | 0.62 | – | – |
| | **13**, 0.62 | **13a**, 0.34 | | |
| | **15**, 0.06 | **15a**, 0.11 | | |
| | **17**, 0.13 | **17a**, 0.10 | | |
| | | **18a**, 0.07 | | |
| $5_1^-$ | 0.80 | 0.55 | 0.31 | 0.16 |
| | **13**, 0.75 | **13a**, 0.43 | **13d**, 0.21 | **1l**, 0.06 |
| | **15**, 0.05 | **15a**, 0.12 | **15d**, 0.10 | **3l**, 0.05 |
| | | | | **8l**, 0.05 |
| $6_1^-$ | 0.77 | 0.59 | 0.37 | 0.13 |
| | **13**, 0.27 | **13a**, 0.11 | **13d**, 0.06 | **17g**, 0.07 |
| | **17**, 0.45 | **17a**, 0.28 | **17d**, 0.17 | **19g**, 0.06 |
| | **20**, 0.05 | **18a**, 0.11 | **18d**, 0.06 | |
| | | **19a**, 0.09 | **19d**, 0.08 | |
| $7_1^-$ | 0.90 | 0.57 | 0.35 | 0.33 |
| | **17**, 0.64 | **13a**, 0.51 | **13d**, 0.07 | **1l**, 0.13 |
| | **18**, 0.05 | **15a**, 0.07 | **13n**, 0.06 | **3l**, 0.09 |
| | **19**, 0.08 | **1m**, 0.16 | **1n**, 0.15 | **8l**, 0.11 |
| | **20**, 0.07 | | **3n**, 0.07 | |
| | **22**, 0.06 | | | |
| $9_1^-$ | 0.98 | 0.64 | 0.28 | 0.34 |
| | **14**, 0.81 | **13a**, 0.51 | **13d**, 0.07 | **2l**, 0.13 |
| | **20**, 0.17 | **15a**, 0.05 | **17d**, 0.07 | **5l**, 0.16 |
| | | **17a**, 0.08 | **1n**, 0.09 | **8l**, 0.0 5 |
| | | | **13n**, 0.05 | |

work we observe cascades on top of the $\nu(g_{7/2}h_{11/2})_{9^-}$ configuration in $^{94}$Sr and $^{96}$Sr. They have higher excitation energies than analogous levels in Zr isotopes due to the higher $\pi g_{9/2}$ energy at Z=38 than at Z=40.

### F. Medium-spin, positive-parity excitations in Sr

The lowest two-q.p., fully-aligned excitations of positive parity in the discussed nuclei correspond to the $(g_{9/2})^2_{8^+}$ and $(f_{5/2})^2_{4^+}$ proton as well as the $(d_{5/2})^2_{4^+}$ and $(g_{7/2})^2_{6^+}$ neutron configurations. Four-q.p., fully-aligned configurations can be obtained by coupling the basic $(g_{9/2})^2_{8^+}$ two-q.p. proton configuration with other two-q.p. levels. Studies of these levels may provide further information on the population of the crucial $\nu g_{7/2}$ and $\pi g_{9/2}$ shells. In previous sections we found that up to N=56 the population of the $\nu g_{7/2}$ shell is low. The low population of the $\nu 1g_{7/2}$ shell at N=51 was also reported in Refs. [62, 117]. Interestingly, in a recent study of $^{97}$Zr$_{57}$ [35] numerous $7/2^+$ levels are reported, suggesting an increased population of this orbital at N=57.

Figure 22 shows energies of medium-spin, positive-parity levels in Sr and Zr isotopes, which correspond to spherical configurations (spin-parity assignments to some of the levels shown are tentative). Figure 22 provides some interesting observations:

(i) excitation energies are generally lower in Zr nuclei than in their Sr isotones

(ii) energies of two- and four-quasiparticle configurations in Sr isotopes decrease with the increasing N

(iii) in contrast to Sr nuclei the energies in Zr isotopes increase with the increasing N (medium-spin, spherical configurations are not known in $^{98}$Zr)

Lower excitation energies in Zr isotopes are most likely due to higher population of the $\pi g_{9/2}$ shell in Zr than in

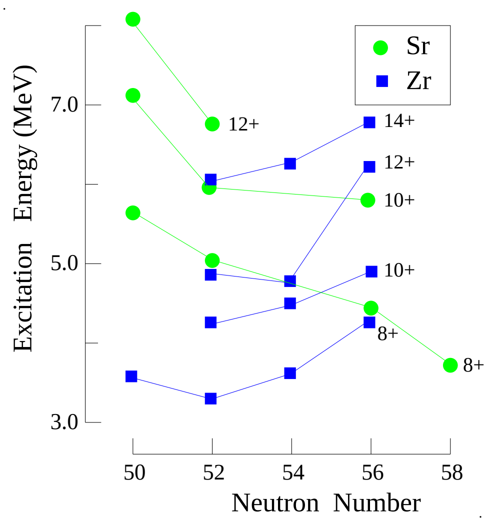


FIG. 22: Experimental excitation energies of medium-spin, positive-parity levels in Sr and Zr isotopes. The data are taken from this work and Refs. [4, 116, 118].

Sr nuclei. However, the decrease of the $8^+$ energy as a function of the neutron number in Sr isotopes and its increase in Zr isotopes suggest the involvement of neutron levels. The N=56 shell closure at Z=40 is stronger than at Z=38 (see Fig. 8). Consequently, the population of the $\nu g_{7/2}$ shell may be higher in Sr compared to Zr isotopes. Due to the SOP mechanism the higher population of the $\nu g_{7/2}$ shell may result in lower excitation of the $(g_{9/2})^2_{8+}$ level in Sr nuclei. The strong closure at N=56 in Zr isotopes is responsible for the energy increases seen in Fig. 22. It seems that higher population of the $\pi g_{9/2}$ shell in Zr isotopes, expected to increase the collectivity is not sufficient to override the Z=40 shell closure effect.

Finally, let us comment on the high-K, 2-q.p. band in $^{96}$Sr. In Ref. [48] the $(6^+)$ level at 2533.1 keV in $^{98}$Sr was interpreted as the parallel coupling of the $9/2^+[404]$ and $3/2^+[411]$ neutron orbitals. Their $(3^+)$ antiparallel coupling was proposed in $^{98}$S at 1837.8 keV [87], defining rather large Gallagher-Moszkowski interaction of 696 keV [48]. The rotational band of ΔI=1 transitions on top of the 2533.1 keV level in $^{98}$Sr is very similar to the band on top of the 3605.4-keV, $(6^+)$ level in $^{96}$Sr. Assuming the $\nu 9/2^+[404] \otimes 3/2^+[411]$ configuration of the 3605.4-keV level one may expect the antiparallel $3^+$ coupling in $^{96}$Sr above 2.9 MeV. Such a level could be populated in $\beta$ decay of the $2^+$ ground state of $^{96}$Rb. A possible candidate is the 3064.8-keV level [51], as suggested by our triple coincidence data, which shows a weak 145 keV feeding of this level.

The 1071-keV drop of the proposed $\nu(9/2^+[404] \otimes 3/2^+[411])_{6^+}$ configuration between $^{96}$Sr and $^{98}$Sr suggests that both orbitals involved are closer to the Fermi surface at N=60 than at N=58, which coincides with the picture in Figs. 10 (d) and (e). This supports further the involvement of the $\nu(9/2^+[404]$ extruder in the development of strongly deformed configurations around N=60.

## IV. SUMMARY AND PERSPECTIVES

In summary, excited levels in $^{90-96}$Sr were studied using data from measurements of $\gamma$ rays following spontaneous fission of $^{252}$Cf and neutron-induced fission of $^{235}$U, performed with Gammasphere and EXILL multidetector arrays, respectively. In total 23 new levels with 30 new or corrected decays and 39 new or improved spin-parity assignments were obtained in these nuclei. In $^{96}$Sr, we found the $2^+_2 \rightarrow 0^+_2$, E2 transition in the deformed band and determined its rate of B(E2)≥38(8)W.u. A mechanism involving the $\nu 9/2^+[404]$ extruder was proposed to explain the origin of $0^+$ excitations and the evolution of deformation in Sr isotopes. A new classification of $2^+$ excitations in the region, supported by the large-scale shell-model calculations (see Fig. 14) was presented, indicating that most of the $2^+$ excitations in the studied nuclei are dominated by single-particle excitations, which do not contribute significantly to a development of quadrupole collectivity. These s.-p. excitations provide, however, a "skeleton" for other collective excitations such as $\gamma$ vibrations and mixed- parity excitations. The latter are now proposed also in Sr isotopes. The LSSM calculations describe well the $3^+$ excitations characteristic of these modes. However, the calculation do not reproduce the systematic of $3^-$ levels in Sr isotopes above N=92, suggesting an admixture of collective effects setting in with the increasing neutron number.

Further experimental studies of Sr isotopes are of high interest. First of all, measurements of nucleon-pair transfer to and from $0^+_i$ and $2^+_i$ excitations in the A≈100 region should be performed, to verify their structures proposed in this work.

The authors thank the technical services of the ILL, LPSC and GANIL for supporting the EXILL campaign. The Exogam collaboration and the INFN Legnaro are acknowledged for the loan of Ge detectors. This material is based upon work supported by the U.S. Department of Energy, Office of Science, Office of Nuclear Physics, under contract number 1 DE-AC02-06CH11357.

[1] W. Urban, T. Rząca-Urban, J. Wiśniewski, I. Ahmad, A.G. Smith, and G.S. Simpson, Phys. Rev. C, **99**, 064325 (2019).
[2] K. Heyde, J.L. Wood, Rev. Mod. Phys. **83**, 1467 (2011).
[3] W. Urban, M. Jentschel, R.F. Casten, J. Jolie, Ch. Bernards, B. Maerkisch, Th. Materna, P. Mutti, L. Próchniak, T. Rząca-Urban, G.S. Simpson, V. Werner,and S. Ahmed, Phys. Rev. C **87**, 031304(R) (2013).
[4] Evaluated Nuclear Structure Data File (ENSDF),

*www.nndc.bnl.gov/ensdf/*.
[5] F. Schussler, J.A. Pinston, E. Monnand, A. Moussa, G. Jung, E. Koglin, B. Pfeiffer, R.V.F.Janssens, and J.van Klinken, Nucl. Phys. **A339**, 415 (1980).
[6] J.F. Sharpey-Schafer, S.M. Mulins, R.A. Bark, J. Kau, F. Komati, E.A. Lawrie, J.J. Lawrie, T.E. Madiba, P. Maine, A. Minkova, S.H.T. Murray, N.J. Ncapayi, and P.A. Vymers, Eur. Phys. J. A **47**: 5 (2011).
[7] J.F. Sharpey-Schafer, R.A. Bark, S.P. Bvumbi, T.R.S. Dinoko, and S.N.T. Majola, Eur. Phys. J. A **55**: 15 (2019).
[8] W. Urban, T. Rząca-Urban, A.G. Smith, G.S. Simpson, and J.P. Greene, Pys. Rev. C **102**, 064321 (2020).
[9] B.R. Mottelson, and S.G. Nilsson, Phys. Rev. 99, 1615 (1955).
[10] F. Barranco, G.F. Bertsch, R.A. Broglia, and E. Vigezzi, Nucl. Phys **A 512**, 253 (1990).
[11] R.A. Broglia, F. Barranco, G.F. Bertsch, and E. Vigezzi, Phys. Rev. C **49**, 552 (1994).
[12] K. Matsuyanagi, M. Matsuo, T. Nakatsukasa, K. Yoshida, N. Hinohara, and K. Sato, Phys. Scr. **91**, 063014 (2016).
[13] V. Paar, Nucl. Phys. A **211**, 29 (1973); Phys. Lett. B **39**, 587 (1972).
[14] A. Kuriyama, T. Maromuri, K. Matsuyanagi, Prog. Theor. Phys. **47**, 498 (1972); Prog. Theor. Phys. **51**, 779 (1974).
[15] A. Kuriyama, T. Maromuri, K. Matsuyanagi, R. Okamoto, Prog. Theor. Phys. **53**, 489 (1975).
[16] T. Rząca-Urban, W.Urban, A.G.Smith, I.Ahmad, F.Nowacki, and K. Sieja, Phys. Rev. C **88**, 034302 (2013).
[17] J. Wiśniewski, W. Urban, M. Czerwiński, J. Kurpeta, A. Płochocki, M. Pomorski, T. Rząca-Urban, K. Sieja, L. Canete, T. Eronen, *et al.*, Phys.Rev. C **100**, 054331 (2019).
[18] T. Rząca-Urban, K. Sieja, W. Urban, F. Nowacki, J.L. Durell, A.G. Smith, and I. Ahmad, Phys. Rev. C **79**, 024319 (2009).
[19] W. Urban, J.L. Durell, W.R. Phillips, A.G. Smith, M.A. Jones, I. Ahmad, A.R. Barnett, M. Bentaleb, S.J. Dorning, M.J. Leddy, E. Lubkiewicz, L.R. Morss, T. Rząca-Urban, R.A. Sareen, N. Schulz, and B.J. Varley, Z.Phys. A **358**, 145 (1997).
[20] I-Yang Lee, Nucl. Phys. A **520**, c641 (1990).
[21] M. Jentschel, A. Blanc G. deFrance, U. Köster, S. Leoni, P. Mutti, G.S. Simpson, T. Soldenr, C. Ur, W. Urban, and the EXILL collaboration, JINST **12**, P11003 (2017).
[22] H. Naidïa, F. Nowacki, B. Bounthong, M. Czerwiński, T. Rząca-Urban, T. Rogiński, W. Urban, J. Wiśniewski, A.G. Smith, J.F. Smith, G.S. Simpson, I. Ahmad, and J.P. Greene, Phys. Rev. C **95**, 064303 (2017).
[23] W.Urban, , A. Abramuk, A. Blanc[b], M. Czerwiński, G. de France, M. Jentschel, U. Köster, S. Leoni, P. Mutti, T. Rząca-Urban, G.S. Simpson, C.A. Ur, and J. Wiśniewski, JINST (2021), to be published.
[24] W.L. Talbert, Jr., F.K. Wohn, L.J. Alquist, and C.L. Duke, Phys. Rev. C **23**, 1726 (1981).
[25] N. Fotiades, J.A. Cizewski, K.Y. Ding, R. Krücken, J.A. Becker, L.A. Bernstein, K. Hauschild, D.P. McNabb,W. Younes, P. Fallon, I.Y. Lee, and O. Macchiavelli, Phys. Scr. **T88**, 127 (2000).
[26] E.A. Stefanova, M. Danchev, R. Schwengner, D. L. Balabanski, M. P. Carpenter, M. Djongolov, S. M. Fischer, D. J. Hartley, R. V. F. Janssens, W. F. Mueller, D. Nisius, W. Reviol, L. L. Riedinger, and O. Zeidan, Phys. Rev. C **63**, 064315 (2002).
[27] S.K. Basu, and E.A. Mccutchan, Nucl. Data Sheets **165**, 1 (2020).
[28] C.M. Baglin, Nucl. Data Sheets **113**, 2187 (2012).
[29] I. Ahmad, and W.R. Phillips, Rep. Prog. Phys. **58**, 1415 (1995).
[30] A. Kumar, and M.R. Guyne, Phys. Rev. C **32**, 2116 (1985).
[31] J. Dobaczewski, Proc. Int. Conf. on Nucl. Struct. Physics, Cocoyoc 1988, ed. R. Casten, A. Frank, M. Moshinski and S. Pittel, World Scientific 1988, pp 227-242.
[32] J. Skalski, P.-H. Heenen, and P. Bonche, Nucl. Phys. **A559**, 221 (1993).
[33] W. Urban, J.L. Durell, A.G. Smith, W.R. Phillips, M.A. Jones, B.J. Varley, T. Rzça-Urban, I. Ahmad, L.R.Morss, M. Bentaleb, and N. Schulz, Nucl. Phys **A689**, 605 (2001).
[34] T.R. Werner, J. Dobaczewski, M.W. Guidry, W. Nazarewicz, and J.A. Sheikh, Nucl. Phys. **A578**, 1 (1994).
[35] T. Rząca-Urban, W. Urban, M. Czerwński, J. Wiśniewski, A. Blanc, H. Faust, M. Jentschel, P. Mutti, U. Köster, T. Soldner, G. de France, G.S. Simpson, and C.A. Ur, Phys. Rev. C **98**, 064315 (2018).
[36] J.H. Hamilton, A.V.Ramayya, S.J. Zhu, G.M. Ter-Akopian, Yu.Ts. Oganessian, J.D.Cole, J.O.Rasmussen, and M.A.Stoyer, Prog. Nucl. Part. Phys. **35**, 635 (1995).
[37] J.-M. Régis, J. Jolie, N. Saed-Samii, N. Warr, M. Pfeiffer, A. Blanc, M. Jentschel, U. Köster, P. Mutti, T. Soldner, G. S. Simpson, F. Drouet, A. Vancraeyenest, G. de France, E. Clément, O. Stezowski, C. A. Ur, W. Urban, *et al*, Phys. Rev. C **95**, 054319 (2017).
[38] G. Jung, B. Pfeiffer, L. J. Alquist, H. Wollnik, P. Hungerford, S. M. Scott, and W. D. Hamilton, Phys. Rev. C **22**, 252 (1980).
[39] A. Negret, and A.A. Sonzogni, Evaluated Nuclear Structure Data File (2011).
[40] I. Tsekhanovich, G. S. Simpson, W. Urban, J. A. Dare, J. Jolie, A. Linnemann, R. Orlandi, A. Scherillo, A. G. Smith, T. Soldner, B. J. Varley, T. Rzca-Urban, A. Zomaniec, O. Dorvaux, B. J. P. Gall, B. Roux, and J. F. Smith, Phys. Rev. C **78**, 011301(R) (2008).
[41] S. Cruz, K. Wimmer, S.S. Bhattacharjee, P.C. Bender, G. Hackman, R. Krucken, F. Ames, C. Andreoiu, R.A.E. Austin, C.S. Bancroft, *et al.*, Rev. C **102**, 024335 (2020).
[42] G. Jung, PhD Thesis, (1980).
[43] E. Clément, M. Zieliska, A. Görgen, W. Korten, S. Péru,J. Libert, H. Goutte, S. Hilaire, B. Bastin, C. Bauer, A. Blazhev, *et al*, Phys. Rev. Lett. **116**, 022701 (2016).
[44] E. Clément, M. Zieliska, S. Péru, H. Goutte, S. Hilaire, A. Görgen, W. Korten, D.T. Doherty, B. Bastin, C. Bauer, *et al*, Phys. Rev. C **94**, 054326 (2016).
[45] S. Cruz, P.C. Bender, R. Krucken, K. Wimmer, F. Ames, C. Andreoiu, R.A.E. Austin, C.S. Bancroft, R. Braid, T. Bruhn, *et al.*, Phys. Lett. B **786**, 94 (2018).
[46] S. Cruz, K.Wimmer, P.C. Bender, R. Krucken, G. Hackman, F. Ames, C. Andreoiu, R.A.E. Austin, C.S. Bancroft, R. Braid, *et al.*, Rev. C **100**, 054321 (2019).

[47] M.A.C. Hotchkis, J.L. Durell, J.B. Fitzgerald, A.S. Mowbray, W.R. Phillips, I. Ahmad, M.P. Carpenter, R.V.F. Janssens, T.L. Khoo, E.F. Moore, L.R. Morss, Ph. Benet, and D.Ye, Nucl. Phys. A **530**, 111 (1991).
[48] J.L. Durell, T.J. Armstrong, and W. Urban, Eur. Phys. J. A **20**, 97 (2004).
[49] A. G. Smith, J. L. Durell, W. R. Phillips, W. Urban, P. Sarriguren, and I. Ahmad, Phys. Rev. C **86**, 014321 (2012).
[50] C.Y. Wu, H. Hua, D. Cline, A.B. Hayes, R. Teng, R.M. Clark, P. Fallon, A. Goergen, A.O. Macchiavelli, and K. Vetter, Phys. Rev. C **70**, 064312 (2004).
[51] D. Abriola(a), and A.A. Sonzogni, Nucl. Data Sheets **109**, 2501 (2008).
[52] P. Federman and S. Pittel, Phys. Lett. B **69**, 385 (1977); Phys. Lett. B **77**, 29 (1978); Phys.Rev. C **20**, 820 (1979).
[53] C. Kremer, S. Aslanidou, S. Bassauer, M. Hilcker, A. Krugmann, P. von Neumann-Cosel, T. Otsuka, N. Pietralla, V. Yu. Ponomarev, N. Shimizu, M. Singer, G. Steinhilber, T. Togashi, Y. Tsunoda, V. Werner, and M. Zweidinger, Phys. Rev. Lett. **117**, 172503 (2016).
[54] Y. Tsunoda, T. Otsuka, N. Shimizu, M. Honma, and Y. Utsuno Phys. Rev. C **89**, 031301(R) (2014).
[55] R.A. Meyer, E. Monnand, J.A. Pinston, F. Schussler, B. Pfeiffer, I. Ragnarsson, H. Lawin, G. Lhersonneau, and K. Sistemich, Nucl. Phys. **A439**, 510 (1985).
[56] B.M. Nyakó, J. Timár , M. Csatlós, Zs. Dombrádi, A. Krasznahorkay, I. Kuti, D. Sohler, T.G. Tornyi, M. Czerwiński, T. Rząca-Urban, W. Urban, P. Bączyk, L. Atanasova, D.L. Balabanski, K. Sieja, A. Blanc, M. Jentschel, U. Köster, P. Mutti, T. Soldner, G. de France, G.S. Simpson, and C.A. Ur, Phys.Rev. C 103, 034304 (2021).
[57] W. Urban, K. Sieja, T. Materna, M. Czerwiński, T. Rząca, C. Fransen, J. Jolie, J.-M. Regis, T. Thomas, and N. Warr, Phys.Rev. C **94** 044328 (2016).
[58] K. Heyde, P. Van Isacker, R.F. Casten, and J.L. Wood, Phys. Lett. B **155**, 303 (1985).
[59] W. Urban, T. Rząca-Urban, A. Złomaniec, G. Simpson, J.L. Durell, W.R. Phillips, A.G. Smith, B.J. Varley, I. Ahmad, and N. Schulz, Eur. Phys. J A **16**, 11 (2003).
[60] W. Urban, J.A. Pinston, J. Genevey, T. Rząca-Urban, A. Złomaniec, G. Simpson, J.L. Durell, W.R. Phillips, A.G. Smith, B.J. Varley, I. Ahmad, and N. Schulz, Eur. Phys. J. A **22**, 241 (2004).
[61] K. Sieja, F. Nowacki, K. Langanke, and G. Martinez-Pinedo Phys. Rev. C **79**, 064310 (2009).
[62] F. Didierjean, D. Verney, G. Duchene, J. Litzinger, K. Sieja, A. Dewald, A. Goasduff, R. Lozeva, C. Fransen, G. de Angelis, S. Aydin, D. Bazzacco, A. Bracco, S. Bottoni, *et al*, Phys. Rev. C **96**, 044320 (2017).
[63] T. Materna, W. Urban, K. Sieja, U. Köster, H. Faust, M. Czerwiński, T. Rząca-Urban, C. Bernards, C. Fransen, J. Jolie, J.-M. Regis, T. Thomas, and N. Warr, Phys. Rev. C **92**, 034305 (2015).
[64] T. Rząca-Urban, K. Sieja, W. Urban, M. Czerwiński, A. Blanc, M. Jentschel, P. Mutti, U. Köster, T. Soldner, G. de France, G.S. Simpson, and C.A.Ur, Phys. Rev. C **95**, 064302 (2017).
[65] K. Sieja, in preparation.
[66] F. Buchinger, E.B. Ramsay, E. Arnold, W. Neu, R. Neugart, K. Wendt, R.E. Silverans, P. Lievens, L. Vermeeren, D. Berdichevsky, R. Fleming, D.W.L. Sprung, and G. Ulm, Phys.Rev. C **41**, 2883 (1990); Erratum Phys.Rev. C42, 2754 (1990).
[67] N. Gavrielov, A. Leviatan, and F. Iachello, Phys. Rev. C **99**, 064324 (2019).
[68] J.E. Garcia-Ramos, and K. Heyde, Phys. Rev. C **100**, 044315 (2019).
[69] P.E. Garrett, J.Phys.G. Nucl.Part.Phys. **27**, R1 (2001).
[70] P.E. Garrett, W.D. Kulp, J.L. Wood, D. Bandyopathayay, S. Choudry, D. Dashodroj, S.R. Lesher, M.T. McEllistrem, M. Mynk, J.N. Orc, and S.W. Yates, Phys. Rev. Lett **103**, 062501 (2009).
[71] A. Leviatan, N. Gavrielov, J.E. Garcia-Ramos, and P. Van Isacker, Phys. Rev. C **98**, 031302(R) (2018).
[72] T. Togashi, Y. Tsunoda, T. Otsuka, and N. Shimizu, Phys.Rev.Lett. **117**, 172502 (2016).
[73] P.E. Garrett, L. Makhathini, R.A. Bark, T.R. Rodriguez, S. Valbuena, V. Bildstein, T.D. Bucher, C. Burbadge, R. Dubey, T. Faestermann, *et al.*, Phys. Lett. B **809**, 135762 (2020).
[74] G.F. Bertsch, Eur. Phys. J. A **55** : 248 (2019).
[75] P.F. Bortignon, and R.A. Broglia, Eur. Phys. J. A **52** : 280 (2016).
[76] C. Walz, H. Fujita, A. Krugmann, P. von Neumann-Cosle, N. Pietrala, V. Yu. Ponomarev, A. SheikhObeid, and J. Wambach, Phys. Rev. Lett **106**, 062501 (2011).
[77] B. Elman, A. Gade, D. Weisshaar, D. Barofsky, D. Bazin, P.C. Bender, M. Bowry, M. Hjorth-Jensen, K.W. Kemper, *et al*, Phys. Rev. C **96**, 044332 (2017).
[78] A. Chester, G.C. Ball, R. Caballero-Folch, D.S. Cross, S. Cruz, T. Domingo, T.E. Drake, A.B. Garnsworthy, G. Hackman, S. Hallam, *et al.*, Phys.Rev. C **96**, 011302 (2017).
[79] J. Dudouet, A.Lemasson, G. Duchene, M. Rejmund, E. Clement, C. Michelagnoli, F. Didierjean, A. Korichi, G. Maquart, O. Stezowski, C. Lizarazo, *et al.*, Phys Rev. Lett. **118**, 162501 (2017).
[80] K. Heyde, J. Jolie, R. Fossion, S. De Baerdemacker, and V. Hellemans, Phys.Rev. C **69**, 054304 (2004).
[81] R.F. Casten, and E.A. McCutchan, J. Phys. G: Nucl. Part. Phys. **34**, R285 (2007).
[82] S. Naimi, G. Audi, D. Beck, K. Blaum, Ch. Bohm, Ch. Borgmann, M. Breitenfeldt, S. George, F. Herfurth, A. Herlert, M. Kowalska, *et al.*, Phys Rev. Lett. **105**, 032502 (2010).
[83] I. Mukul, C.Andreoiu, J.Bergmann, M.Brodeur, T.Brunner, K.A.Dietrich, T.Dickel, I.Dillmann, E.Dunling, D.Fusco, *et al.*, Phys. Rev. C **103**, 044320 (2021).
[84] R.B. Cakirli, R.F. Casten, R. Winkler, K. Blaum, and M. Kowalska, Phys. Rev. Lett. **102**, 082501 (2009).
[85] R.B. Cakirli, R.F. Casten, and K. Blaum, Phys. Rev. C **82**, 061306(R) (2010).
[86] R. Rodriguez-Guzman, P. Sarriguren, L.M. Robledo, and S. Perez-Martin, Phys. Lett. B **691**, 202 (2010).
[87] G.Lhersonneau, B.Pfeiffer, R.Capote, J.M.Quesada, H.Gabelmann, K.-L.Kratz, and the ISOLDE Collaboration, Phys.Rev. C **65**, 024318 (2002).
[88] J.K. Hwang, A.V. Ramayya, J.H. Hamilton, D. Fong, C.J. Beyer, P.M. Gore, Y.X. Luo, J.O. Rasmussen, S.C. Wu, I.Y. Lee, C.M. Folden, III, P. Fallon, *et al.*, Phys. Rev. C **67**, 054304 (2003).
[89] A. Złomaniec, H. Faust, J. Genevey, J.A. Pinston, T. Rząca-Urban, G.S. Simpson, I. Tsekhanovich, and W. Urban, Phys. Rev. C 72, 067302 (2005).

[90] W. Urban, M. Czerwiński, J. Kurpeta, T. Rząca-Urban, J. Wiśniewski, T. Materna, Ł.W. Iskra, A. G. Smith, I. Ahmad, A. Blanc, H. Faust, U. Köster, M. Jentschel, P. Mutti, T. Soldner, G. S. Simpson, J.A. Pinston, G. de France, C.A. Ur, *et al.*, Phys. Rev. C **96**, 044333 (2017).

[91] A. Esmaylzadeh, J.-M. Regis, Y.H. Kim, U. Köster, J. Jolie, V. Karayonchev, L. Knafla, K. Nomura, L.M. Robledo, and R. Rodriguez-Guzman, Phys.Rev. C **100**, 064309 (2019).

[92] A. Guessous, N. Schulz, M. Bentaleb, E. Lubkiewicz, J.L. Durell, C.J. Pearson, W.R. Phillips, J.A. Shannon, W. Urban, B.J. Varley, I. Ahmad, C.J. Lister, L.R. Morss, K.L. Nash, C.W. Williams, and S. Khazrouni, Phys. Rev. C **53**, 1191 (1996).

[93] J.A. Shannon, W.R. Phillips, J.L. Durell, B.J. Varley, W. Urban, C.J. Pearson, I. Ahmad, C.J. Lister, L.R. Morss, K.L. Nash, C.W. Williams, N. Schulz, E. Lubkiewicz, and M. Bentaleb, Phys. Lett. B **336**, 136 (1994).

[94] A. Guessous, N. Schulz, W.R. Phillips, I. Ahmad, M. Bentaleb, J.L. Durell, M.A. Jones, M. Leddy, E. Lubkiewicz, L.R. Morss, R. Piepenbring, A.G. Smith, W. Urban, and B.J.Varley, Phys. Rev. Lett. **75**, 2280 (1995).

[95] N.V. Zamfir, and R.F. Casten, Phys. Lett. B bf 260, 265 (1991).

[96] E.A. McCutchan, D. Bonatsos, N.V. Zamfir, and R.F.Casten, Phys. Rev. C **76**, 024306 (2007).

[97] R.F. Casten, R.B. Cakirli, D. Bonatsos, and K. Blaum, Phys. Rev. C **102**, 054310 (2020).

[98] A. Poves, F. Nowacki, and Y. Alhassid, Phys. Rev. C **101**, 054307 (2020).

[99] I.N. Gratchev, G.S. Simpson, G. Thiamova, M. Ramdhane, K. Sieja, A. Blanc, M. Jentschel, U. Köster, P. Mutti, T. Soldner, G. de France, C.A. Ur, and W. Urban, Phys. Rev. C **95**, 051302 (2017).

[100] W. Urban, T. Rząca-Urban, J. Wiśniewski, A.G. Smith, G.S. Simpson, and I. Ahmad, Phys. Rev. C **100**, 014319 (2019).

[101] K. Sieja, T.R. Rodriguez, K. Kolos and D. Verney, Phys. Rev. C **88**, 034327 (2013).

[102] S.W. Yates, Journal of Radioanalytical and Nuclear Chemistry, **265**, 291 (2005).

[103] N. Pietralla, P. von Brentano, and A.F. Lisetskiy, Prog. Part. Nucl. Phys. **60**, 225 (2008).

[104] K. Sieja, G. Martinez-Pinedo, L. Coquard, and N. Pietralla, Phys. Rev. C **80**, 054311 (2009).

[105] V. Werner, D. Belic, P. von Brentano, C. Fransen, A. Gade, H. von Garrel, J. Jolie, U. Kneissl, C. Kohstall, A. Linnemann, A.F. Lisetskiy, N. Pietralla, H.H. Pitz, M. Sheck, K.-H. Speidel, F. Stedile, and S.W. Yates, Phys. Lett. **B 550**, 140 (2002).

[106] N. Pietralla, C. Fransen, D. Belic, P. von Brentano, C. Friessner, U. Kneissl, A. Linneman, A. Nord, H.H. Pitz, T. Otsuka, I. Schneider, V. Werner, and I Wiedenhoeven, Phys. Rev. Lett. **83**, 1303 (1999).

[107] N. Pietralla, C. Fransen, P. von Brentano, A. Dewald, A. Fitzler, C. Friessner, and J. Gableske, Phys. Rev. Lett. **84**, 375 (2000).

[108] C. Fransen,N. Pietralla, P. von Brentano, A. Dewald, J. Gableske, A. Gade, A. Lisetskiy, and V. Werner, Phys. Lett. B **508**, 219 (2001).

[109] C. Fransen, N. Pietralla, Z. Ammar, D. Bandyopadhyay, N. Boukharouba, P. von Brentano, A. Dewald, J. Gableske, A. Gade, J. Jolie, *et al.*, Phys. Rev. C **67**, 024307 (2003).

[110] T. Thomas, V. Werner, J. Jolie, K. Nomura. T.Ahn, N. Cooper, H. Duckwitz, A. Fitzler, C. Fransen, A. Gade, *et al.*, Nucl. Phys. A **947**, 203 (2016).

[111] H. Klein, A.F. Lisetskiy, N. Pietralla, C. Fransen, A. Gade, and P. von Brentano, Phys. Rev. C **65**, 044315 (2002).

[112] K. Heyde, P. von Noyumann-Cosel, and A. Richter, Rev. Mod. Phys. **82**, 2365 (2010).

[113] E.A. Mccutchan, and A.A. Sonzogni, Nucl. Data Sheets **115**, 135 (2014).

[114] T. Rząca-Urban, W. Urban, A. Kaczor, J.L. Durell, M.J. Leddy, M.A. Jones, W.R. Phillips, A.G. Smith, B.J. Varley, I. Ahmad, L.R. Morss, M. Bentaleb, E. Lubkiewicz, and N. Schulz, Eur. Phys. J. A **9**, 165 (2000).

[115] E.T. Gregor, N.N. Arsenyev, M. Scheck, T.M. Shneidman, M. Thurauf, C. Bernards, A. Blanc, R. Chapman, F. Drouet, A.A. Dzhioev, *et al.*, J. Phys. G: Nucl. Part. Phys. **46**, 075101 (2019).

[116] G.S. Simpson, J.A. Pinston, D. Balabanski, J. Genevey, G. Georgiev, J. Jolie, D.S. Judson, R. Orlandi, A. Scherillo, I. Tsekhanovich, W. Urban, and N. Warr, Phys. Rev. C **74**, 064308 (2006).

[117] D.K. Sharp, B.P. Kay, J.S. Thomas, S.J. Freeman, J.P. Schiffer, B.B. Back, S. Bedoor, T. Bloxham, J.A. Clark, C.M. Deibel, *et al.*, Phys. Rev. C **87**, 014312 (2013).

[118] D. Pantelica, I.Gh. Stefan, N. Nica, M.-G. Porquet, G. Duchene, A. Astier, S. Courtin, I. Deloncle, F. Hoellinger, A. Bauchet, *et al.*, Phys. Rev. C **72**, 024304 (2005).